

Thermal role of bound states and resonances in scalar QFT

Subhasis Samanta*

*Institute of Physics, Jan-Kochanowski University,
ul. Uniwersytecka 7, 25-406 Kielce, Poland.*

Francesco Giacosa†

*Institute of Physics, Jan-Kochanowski University,
ul. Uniwersytecka 7, 25-406 Kielce, Poland. and
Institute for Theoretical Physics, J. W. Goethe University,
Max-von-Laue-Str. 1, 60438 Frankfurt, Germany.*

We study the thermal properties of quantum field theories (QFT) with three-leg interaction vertices $g\varphi^3$ and $gS\varphi^2$ (φ and S being scalar fields), which constitute the relativistic counterpart of the Yukawa potential. We follow a non-perturbative unitarized one-loop resummed technique for which the theory is unitary, finite, and well defined for each value of the coupling constant g . Using the partial wave decomposition of two-body scattering we calculate the phase shifts, whose derivatives are used to infer the pressure of the system at nonzero temperature. A $\varphi\varphi$ bound state is formed when coupling g is greater than a certain critical value. As one of the main outcomes, we show that this bound state does not count as *one* state in the thermal gas, since a cancellation with the residual $\varphi\varphi$ interaction typically occurs. The amount of this cancellation depends on the details of the model and its parameters: a variety of possible scenarios is presented. Moreover, even when no bound state occurs, we estimate the role of the interaction (including a resonance in the $gS\varphi^2$ theory), which is in general non-negligible. We also show how the overall effect of interaction, including eventual resonances and bound states, can be formally described by a unique expression that makes use of the phase shift derivative below and above the threshold.

arXiv:2110.14752v1 [hep-ph] 27 Oct 2021

* subhasis.samant@gmail.com

† fgiacosa@ujk.edu.pl

I. INTRODUCTION

The production of hadronic bound states such as deuteron (${}^2\text{H}$), tritium (${}^3\text{H}$), helium-3 (${}^3\text{He}$), helium-4 (${}^4\text{He}$), hypertritium (${}^3_\Lambda\text{H}$) and their antiparticles in high energy collisions has created a lot of interest in the community [1–7]. The temperature at the chemical freezeout is much larger than the binding energies of those bound states. Hence the natural question is that how such weakly bound objects can form in such a hot environment? Moreover, the size of such bound states is usually large compared to the inter-particle spacing of the fireball. It is, therefore, important to understand the mechanism of formation of those bound states in a thermal system. Further, a whole new class of X , Y and Z resonances are observed in the QCD spectrum which are not predicted by the quark model; see [8] and references therein. Some of these resonances can be mesonic molecular bound states. Experimentally observed pentaquarks [9] can also be understood as molecular objects.

Two successful phenomenological models describing the production of bound states in high energy collisions are discussed in the literature: the thermal model [10–15] and the coalescence model [16–29]. In the thermal model, bound states are formed directly from the source according to the corresponding probability at a given temperature T . On the other hand, the coalescence model works in a two-step process: first, nucleons are produced from a fireball and, second, the bound states (such as nuclei) are formed long after the emission nucleons when the relative momenta of the nucleons become small. Along the same line, conventional mesons, such as pions and kaons, etc. are directly produced, while molecular states emerge as a secondary product. Till now, it is not clear which assumption is correct, although both models describe the production yields of bound states in high energy collisions quite well. Transport [30] and hybrid dynamical [31] models are also applied to describe bound states.

In Ref. [32], we investigated how to include bound states in a thermal gas in the context of quantum field theory (QFT) by using a scalar $\lambda\varphi^4$ interaction (λ being the dimensionless coupling), which corresponds to a delta-potential in the non-relativistic limit. For that (relatively simple) QFT, it was possible to consider only the s -channel Feynman diagrams. The temperature dependence was incorporated by using the phase-shift (or S -matrix) approach. For $\lambda < 0$ (for which attraction occurs) and $|\lambda|$ above a certain critical value, a bound state forms. It was shown that this bound state is relevant at nonzero temperature, but it counts less than what a single state with the same mass would contribute since a partial cancellation with the residual $\varphi\varphi$ interaction is non-negligible. Note, this is in partial agreement with the quantum mechanical approach of Ref. [14], where a similar (but even more pronounced) cancellation was shown to occur.

A natural continuation of the work in Ref. [32] is to investigate the role of bound states in more complex QFTs, that go beyond the simple contact interaction. The next step is then to consider scalar theories that correspond to the Yukawa interaction, in which, besides the s -channel, also the t -channel and u -channel Feynman diagrams must be included. The simplest of such theories contains the interaction $g\varphi^3$, in which the exchanged particle is of the same type as the scattering ones. The interaction is always attractive (for any value of the coupling constant g) and, if strong enough, a bound state forms. The t - and the u - exchange channels are crucial for the attraction and thus for the formation of the bound state and generate also a left-hand cut in the complex plane, that must be properly taken into account in the unitarized version of the theory.

At nonzero T the bound state (if it forms) must be included as an additional state in the thermal gas: its effect is typically partially cancelled by the residual $\varphi\varphi$ interaction, in a way that resembles the results of Ref. [32]. Yet, this cancellation gets smaller and smaller for increasing coupling, and in the strong coupling limit, one may also see an overall contribution that is even larger than the simple bound state thermal contribution. As expected, the pressure of the system turns out to be continuous as a function of g at any given temperature, showing that the emergence of the bound state does not cause any jump in the pressure, because the abrupt contribution of the bound state is compensated by a jump in the interaction part. Adding a φ^4 -interaction modifies the numerical results but not their qualitative interpretation.

The next interesting theory that we are going to study contains two distinct fields S and φ which interact via a term of the type $gS\varphi^2$. The state S with mass M is exchanged by the two φ -fields. Assuming that $M > 2m$, the fields S corresponds to a resonance with a certain decay width into $\varphi\varphi$ and spectral function, see e.g. Ref. [33] for a detailed description. As well-known, the thermal

properties of the resonance S can be described via $\varphi\varphi$ phase-shift above the threshold, see e.g. Refs. [34–41] and refs. therein. As we shall see, the interaction strongly affects the role of the resonance at nonzero T . Moreover, besides the resonance S , also a bound state can form if g is large enough, making this system quite interesting.

Finally, in all cases mentioned above and in agreement with the postulate of Ref. [32], one can generalize the phase-shift approach for the thermal description of the system by extending it below the threshold. In this case, (eventual) bound-state(s) and resonance(s), if present, are automatically incorporated into the finite- T properties of the thermal gas.

The paper is organized as follows: in Sec. II we briefly present the vacuum's properties of the φ^3 -QFT. Here we discuss scattering phase shifts, unitarization procedure, and the formation of a bound state. Then, in Sec. III we discuss the formalism of the system at finite temperature, including the effect of an additional φ^4 interaction to the QFT potential. Further, in Sec. IV we consider a second state S with the three-leg interaction $S\varphi^2$. Finally, in Sec. V we summarize and conclude the paper.

II. VACUUM PHENOMENOLOGY OF THE SCALAR φ^3 -QFT

In this Section, we describe (some) vacuum properties of the φ^3 theory, with special attention on elements of scattering and on the employed unitarization approach. These properties will be used later on when presenting the results of the system at nonzero T .

A. Lagrangian and amplitudes

The Lagrangian under consideration reads

$$\mathcal{L} = \frac{1}{2} (\partial_\mu \varphi)^2 - \frac{1}{2} m^2 \varphi^2 - \frac{g}{3!} \varphi^3, \quad (1)$$

where the first two terms describe a free particle with mass m and the last term corresponds to the interaction. The coupling constant g has dimension [Energy], therefore the theory is renormalizable [42]. Yet, as we shall comment later on, we shall introduce a non-perturbative unitarization procedure on top of Eq. 1, in such a way to make the theory finite and unitary at each energy.

In the centre of the mass frame the differential cross-section is given by [42]

$$\frac{d\sigma}{d\Omega} = \frac{|A(s, t, u)|^2}{64\pi^2 s}, \quad (2)$$

where $A(s, t, u)$ is the scattering amplitude as evaluated through Feynman diagrams, and s, t and u are Mandelstam variables:

$$s = (p_1 + p_2)^2 \geq 4m^2, \quad (3)$$

$$t = (p_1 - p_3)^2 = -\frac{1}{2}(s - 4m^2)(1 - \cos\theta) \leq 0, \quad (4)$$

$$u = (p_2 - p_3)^2 = -\frac{1}{2}(s - 4m^2)(1 + \cos\theta) \leq 0, \quad (5)$$

where p_1, p_2, p_3 and p_4 are the four-momenta of the particles (p_1, p_2 ingoing and p_3, p_4 outgoing), and θ is the scattering angle. The sum of these three variables is $s + t + u = 4m^2$.

In the particular case of our Lagrangian of Eq. 1, the tree-level scattering amplitude $A(s, t, u)$ takes the form

$$A(s, t, u) = -\frac{g^2}{s - m^2 + i\epsilon} - \frac{g^2}{t - m^2 + i\epsilon} - \frac{g^2}{u - m^2 + i\epsilon}. \quad (6)$$

The amplitude on-shell reads:

$$A(s = 4m^2, 0, 0) = -\frac{g^2}{4m^2 - m^2} - \frac{g^2}{-m^2} - \frac{g^2}{-m^2} = \frac{g^2}{m^2} \left(-\frac{1}{3} + 1 + 1 \right) = \frac{5g^2}{3m^2} > 0, \quad (7)$$

thus attraction wins at the threshold because the attractive t - and u -channels overcome the s -channel repulsion. The s-wave ($l = 0$, where l is the orbital angular momentum) scattering length at tree-level is:

$$ma_0^{\text{SL}} = \frac{1}{32\pi} A(s = 4m^2, 0, 0) = \frac{1}{32\pi} \frac{5g^2}{3m^2} \Rightarrow a_0^{\text{SL}} = \frac{5g^2}{96\pi m^3}. \quad (8)$$

Next, we turn to partial wave expansion [43]:

$$A(s, t, u) = A(s, \theta) = \sum_{l=0}^{\infty} (2l+1) A_l(s) P_l(\cos \theta), \quad (9)$$

where $P_l(\xi)$ with $\xi = \cos \theta$ are the Legendre polynomials with

$$\int_{-1}^{+1} d\xi P_l(\xi) P_{l'}(\xi) = \frac{2}{2l+1} \delta_{ll'}. \quad (10)$$

In general, the l -th wave contribution to the amplitude is given by

$$A_l(s) = \frac{1}{2} \int_{-1}^{+1} d\xi A(s, \theta) P_l(\xi). \quad (11)$$

At tree-level the s-wave amplitude's contribution takes the form:

$$A_0(s) = \frac{1}{2} \int_{-1}^{+1} d\xi A(s, \theta) = -\frac{g^2}{s - m^2} + 2g^2 \frac{\log \left[1 + \frac{s-4m^2}{m^2} \right]}{s - 4m^2}, \quad (12)$$

which at threshold reduces to:

$$A_0(s = 4m^2) = \frac{5g^2}{3m^2}. \quad (13)$$

The s-wave scattering length (at tree-level) a_0^{SL} can be re-obtained as:

$$a_0^{\text{SL}} = \frac{1}{2} \frac{A_0(s = 4m^2)}{8\pi\sqrt{4m^2}} = \frac{1}{32\pi m} \frac{5g^2}{3m^2} = \frac{5g^2}{96\pi m^3}. \quad (14)$$

Note, in order to avoid confusion, we denote with Latin alphabet s -, d -, g - ...as the partial waves with increasing l . On the other hand, we employ calligraphic s , t , and u when referring to the Mandelstam variables. Finally, the calligraphic g refers to the three-leg coupling constant entering into the various Lagrangian(s).

There are two important properties of $A_0(s)$ that need to be discussed since they will be useful later on:

(i) $A_0(s)$ contains a pole for $s = m^2$: this is the pole of the single field in the s -channel, $|A_0(s = m^2)| = \infty$; this simple pole (with nonzero residuum) should be preserved when unitarizing the theory. We assume that the position of the pole is not shifted by loop corrections: this can be achieved by a suitable subtraction.

(ii) $A_0(s)$ diverges for $s = 3m^2$. This is due to the left-hand-cut induced by the t - and the u -channels onto the s -wave. (The residuum is zero, thus no particle corresponds to this divergence). We stress that the existence of the branch cut for $s \leq 3m^2$ is also a consequence of the single-particle pole described in the point (i) [44, 45]. As for (i), we will impose this feature when unitarizing the theory.

We now turn to higher waves. Clearly, $A_{2n+1}(s) = 0$, since each odd wave vanishes. For the d-wave, the corresponding amplitude reads:

$$A_2(s) = \frac{-2g^2}{(s-4m^2)^3} \left(3(8m^4 - 6m^2s + s^2) + (2m^4 + 2m^2s - s^2) \log \left[1 + \frac{s-4m^2}{m^2} \right] \right), \quad (15)$$

which for s close to the threshold is approximated by:

$$A_2(s) \simeq \frac{1}{15} \frac{g^2}{m^6} (s-4m^2)^2. \quad (16)$$

For the g-wave we have:

$$A_4(s) = \frac{-g^2}{3(s-4m^2)^5} \left(-5(46m^4 - 2m^2s - 5s^2)(s-2m^2)(s-4m^2) \right. \\ \left. + 6(74m^8 - 124m^6s + 54m^4s^2 - 4m^2s^3 - s^4) \log \left[1 + \frac{s-4m^2}{m^2} \right] \right), \quad (17)$$

which close to threshold reads:

$$A_4(s) \simeq \frac{g^2}{315m^8} (s-4m^2)^4. \quad (18)$$

Both A_2 and A_4 vanish at the threshold, like any other wave with $l > 0$. The total cross-section reads

$$\sigma(s) = \frac{1}{2} 2\pi \frac{1}{64\pi^2 s} \int_0^\pi |A(s, \theta)|^2 \sin \theta d\theta = \frac{1}{2} 2\pi \frac{1}{64\pi^2 s} \sum_{l=0}^{\infty} 2(2l+1) |A_l(s)|^2, \quad (19)$$

which at threshold reduces to:

$$\sigma(s_{th} = 4m^2) = \frac{1}{2} 2\pi \frac{1}{64\pi^2 s} 2 |A_0(s_{th})|^2 = 8\pi |a_0^{\text{SL}}|^2. \quad (20)$$

As a final step of this subsection, let us introduce the l -th wave phase shifts $\delta_l(s)$ as:

$$\frac{e^{2i\delta_l(s)} - 1}{2i} = \frac{1}{2} \cdot \frac{k}{8\pi\sqrt{s}} A_l(s), \quad (21)$$

where $k = \sqrt{\frac{s}{4} - m^2}$. Note, for s just above threshold we have $\frac{e^{2i\delta_0(s)} - 1}{2i} \simeq \delta_0(s) \simeq ka_0^{\text{SL}}$. In general, the phase-shift $\delta_l(s)$ can be calculated as:

$$\delta_l(s) = \frac{1}{2} \arg \left[1 - \frac{1}{8\pi} \sqrt{\frac{4m^2}{s} - 1} A_l(s) \right]. \quad (22)$$

B. Unitarization

First, we need to introduce the $\varphi\varphi$ loop $\Sigma(s)$. Its imaginary part above the threshold is the usual phase-space kinematic factor (see e.g. Ref. [33]):

$$I(s) = \text{Im} \Sigma(s) = \frac{1}{2} \frac{\sqrt{\frac{s}{4} - m^2}}{8\pi\sqrt{s}} \text{ for } \sqrt{s} > 2m. \quad (23)$$

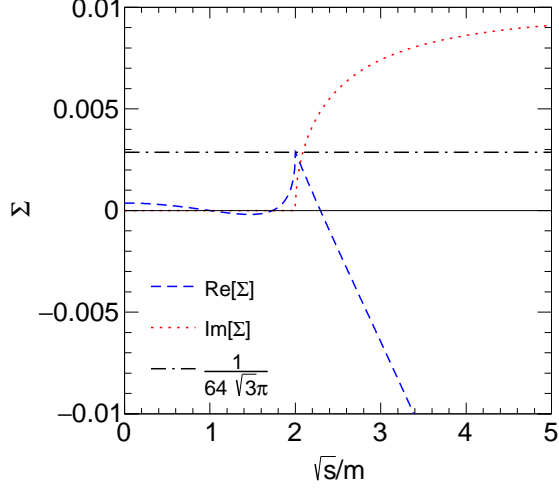


FIG. 1. Energy dependence of the real and imaginary parts of the loop function Σ (see Eq. 24). The value of the Σ at the threshold ($= 1/(64\sqrt{3}\pi)$) is also indicated in this plot.

We use no cutoff, hence the above equation is considered valid up to arbitrary values of the variable s . The imaginary part alone does not fix the form of $\Sigma(s)$ completely. Here, the loop function $\Sigma(s)$ for a complex s is chosen by considering two subtractions:

$$\Sigma(s) = -\frac{(s-m^2)(s-3m^2)}{\pi} \int_{4m^2}^{\infty} \frac{\frac{1}{2} \frac{\sqrt{s'-m^2}}{8\pi\sqrt{s'}}}{(s-s'+i\varepsilon)(s'-m^2)(s'-3m^2)} ds'. \quad (24)$$

The subtractions guarantee that $\Sigma(s = m^2) = 0$ and $\Sigma(s = 3m^2) = 0$. In this way, the choice of $\Sigma(s)$ (i) preserves the pole corresponding to $s = m^2$ (in other words, the tree-level mass is preserved also at the unitarized level) and (ii) assures that the unitarized amplitude diverges at the branch point $s = 3m^2$ generated by the single-particle pole for m^2 along the t and u channels. Interestingly, the same unitarization procedure has been used in the recent work of Ref. [46] dealing with glueball-glueball scattering in an effective dilaton model of Yang-Mills theory.

The real and the imaginary parts of Σ as function of \sqrt{s}/m are shown in Fig. 1. [Note: throughout this paper we consider $m = 1$ in arbitrary unit (a.u.) and all the variables are normalized w.r.t. m .] The function $\text{Re}\Sigma(s)$ vanishes at $\sqrt{s}/m = 1$ and $\sqrt{3}$ as a consequence of the subtractions. In particular, it is positive between $\sqrt{s}/m = \sqrt{3}$ and the threshold $\sqrt{s}/m = 2$, where it reaches the value

$$\Sigma(s = 4m^2) = \frac{3\pi + i \ln\left(\frac{1728(3-i\sqrt{3})^3}{(-36-12i\sqrt{3})^3}\right)}{64\sqrt{3}\pi^2} = \frac{1}{64\sqrt{3}\pi} \approx 0.0028715. \quad (25)$$

In this way a bound states, if existent, has a mass within $(\sqrt{3}m, 2m)$. Above threshold, $\text{Re}\Sigma(s)$ decreases and becomes negative at large \sqrt{s}/m . Conversely, the imaginary part $\text{Im}\Sigma(s)$ is zero (or better infinitesimally small) below threshold, while above threshold it increases according to Eq. (26). It is also useful to re-express the imaginary part $\text{Im}\Sigma(s)$ as:

$$\text{Im}\Sigma(s) = \begin{cases} \frac{1}{2} \frac{\sqrt{\frac{s}{4}-m^2}}{8\pi\sqrt{s}} & \text{for } s > (2m)^2 \\ \epsilon & \text{for } s < (2m)^2 \end{cases}, \quad (26)$$

where $\epsilon \propto \varepsilon$ is an infinitesimal positive quantity.

The unitarized amplitudes are obtained by a resummation of the tree-level amplitudes $A_k(s)$ as:

$$A_k^U(s) = [A_k^{-1}(s) - \Sigma(s)]^{-1}, \quad (27)$$

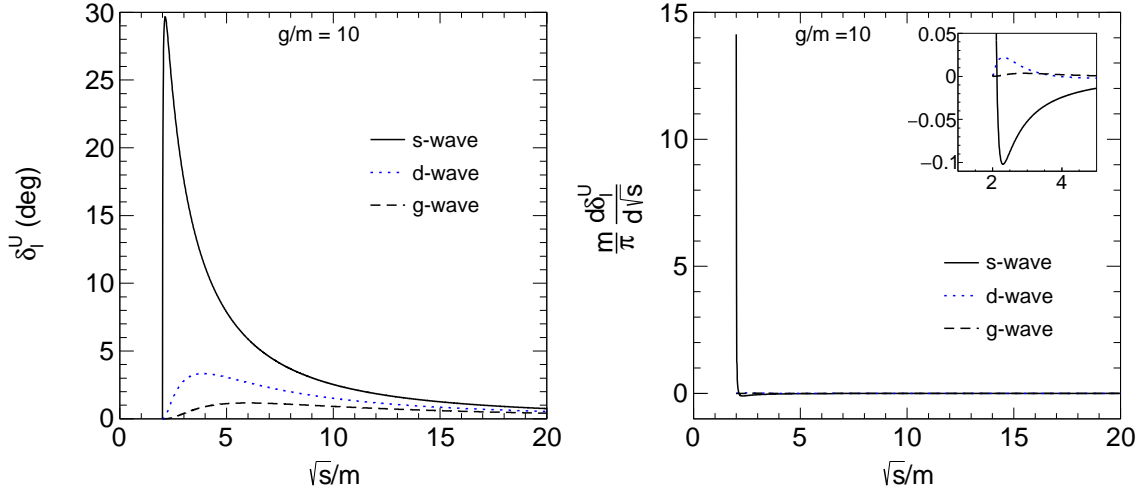


FIG. 2. (Left) Energy dependence of the phase shifts (using Eqs. 27 and 29) for $l = 0, 2, 4$ at $g = 10m < g_c$. (Right) Energy dependence of derivatives of the phase shifts.

leading to the unitarized phase shift

$$\frac{e^{2i\delta_l^U(s)} - 1}{2i} = \frac{1}{2} \cdot \frac{k}{8\pi\sqrt{s}} A_l^U(s), \quad (28)$$

hence:

$$\delta_l^U(s) = \frac{1}{2} \arg \left[1 - \frac{1}{8\pi} \sqrt{\frac{m^2}{s} - \frac{1}{4}} A_l^U(s) \right]. \quad (29)$$

The unitarized scattering length reads:

$$a_0^{U,SL} = \frac{1}{2} \frac{1}{16\pi m} \frac{1}{A_0^{-1}(4m^2) - \Sigma(4m^2)} = \frac{1}{32\pi m} \frac{1}{\frac{3m^2}{5g^2} - \frac{1}{64\sqrt{3}\pi}}. \quad (30)$$

The critical value of g is given by:

$$\frac{3m^2}{5g^2} - \frac{1}{64\sqrt{3}\pi} = 0 \rightarrow \frac{g_c^2}{m^2} = \frac{192\sqrt{3}\pi}{5} \approx 208.95, \quad (31)$$

thus

$$\frac{g_c}{m} \approx 14.4551. \quad (32)$$

For $g = g_c$ the divergence of the scattering length signals the emergence of a bound state just at the threshold, see next subsection.

Note, one can calculate $\delta_l^U(s)$ by using the equivalent expressions

$$\delta_l^U(s) = \frac{1}{2} \arcsin \left[\frac{k}{8\pi\sqrt{s}} \operatorname{Re} [A_l^U(s)] \right] = \frac{1}{2} \arccos \left[1 - \frac{k}{8\pi\sqrt{s}} \operatorname{Im} [A_l^U(s)] \right]. \quad (33)$$

In fact, when unitarization is preserved, the expressions in Eq. (33) and (29) give rise to the same result for the phase shift.

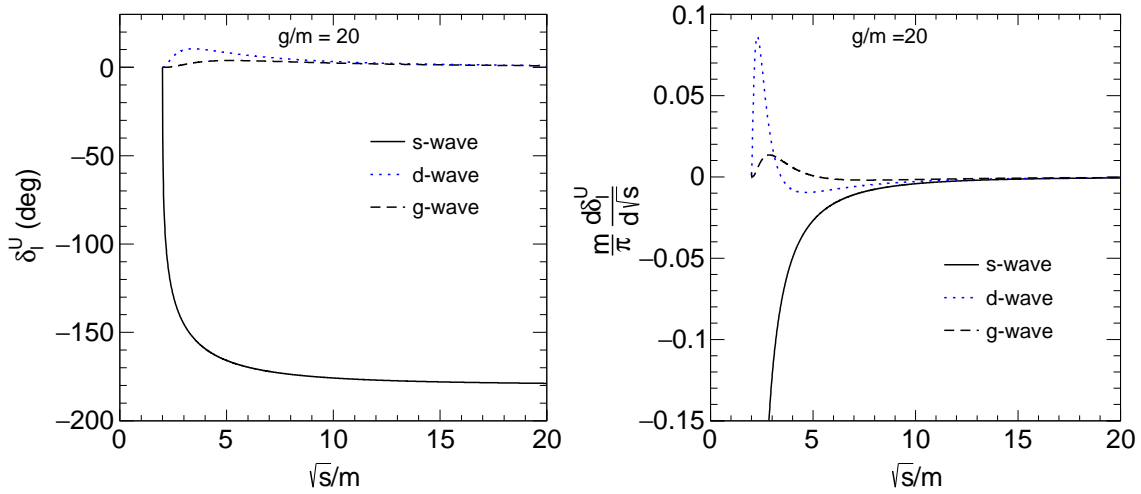


FIG. 3. Energy dependence of the phase shifts (using Eqs. 27 and 29) for $l = 0, 2, 4$ at $g = 20m > g_c$. (Right) Energy dependence of the derivatives of the phase shifts.

Before going into the details of the numerical results of the phase shifts, let us mention the convention adopted in this work. We impose that the phase shifts for any partial waves vanish at threshold:

$$\delta_l^U(s = 4m^2) = 0. \quad (34)$$

Sometimes a different convention is used, according to which the phase space at threshold equals to $n_B\pi$, where n_B is the number of bound states below the threshold [45]. Since the physical quantities are related to the difference and derivative of the phase shifts, the results are unaffected by the choice of the convention of the phase shift at the threshold.

The left panel of Fig. 2 shows the energy dependence of the unitarized phase shifts for s-wave ($l = 0$), d-wave ($l = 2$), and g-wave ($l = 4$) at the coupling $g = 10m < g_c \approx 14.45m$. The s-wave phase shift increases rapidly just above the threshold $\sqrt{s} = 2m$ and then decreases approaching zero at large energies. The d-wave and g-wave show similar behaviour, yet their magnitudes are smaller than that of the s-wave. (Note, the degeneracy factor $(2l + 1)$ is not displayed in Fig. 2). The corresponding phase-shift derivatives are depicted in the right panel of Fig. 2.

Figure 3 shows the same quantities as Fig. 2 but for $g = 20m > g_c$. The s-wave phase shift, shown in the left panel, decreases rapidly above the threshold and saturates at $-\pi$ at large \sqrt{s}/m . This behaviour indicates the presence of a bound state below the threshold, see the next subsection. The phase shifts of d- and g-waves are similar to the previous case. The right panel shows the derivatives of the phase shifts, where it is visible that the s-wave contribution is sizable.

C. Bound state

The bound state equation (s -channel, for s below the threshold) reads:

$$[A_0^{-1}(s) - \Sigma(s)] = 0. \quad (35)$$

In Fig. 4 the mass of the bound state M_B/m is plotted as function of the coupling g . For the critical value $g = g_c + \epsilon \approx 14.45m$ the bound state forms exactly at threshold, and for $g > g_c$ it ranges between $\sqrt{3} < \sqrt{s}/m < 2$, in which $\text{Re}\Sigma(s) > 0$. Note, no bound state is observed in d- and g-waves, the reason being that the tree-level amplitude is non-zero at threshold only in case of the s-wave.

In the left panel of Fig. 5 we show the energy dependence of the s-wave phase shift for $g = 20m > g_c$, in which, in addition to Fig. 3, also the sub-threshold range is displayed. For $\sqrt{s} \approx 1.968 = M_B$ there

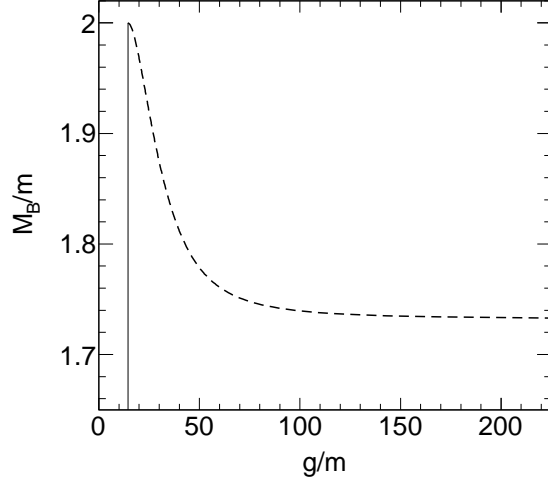


FIG. 4. Variation of the bound state mass (Eq. 35) with the coupling g . The vertical line indicates the critical coupling g_c , for which $M_B = 2m$.

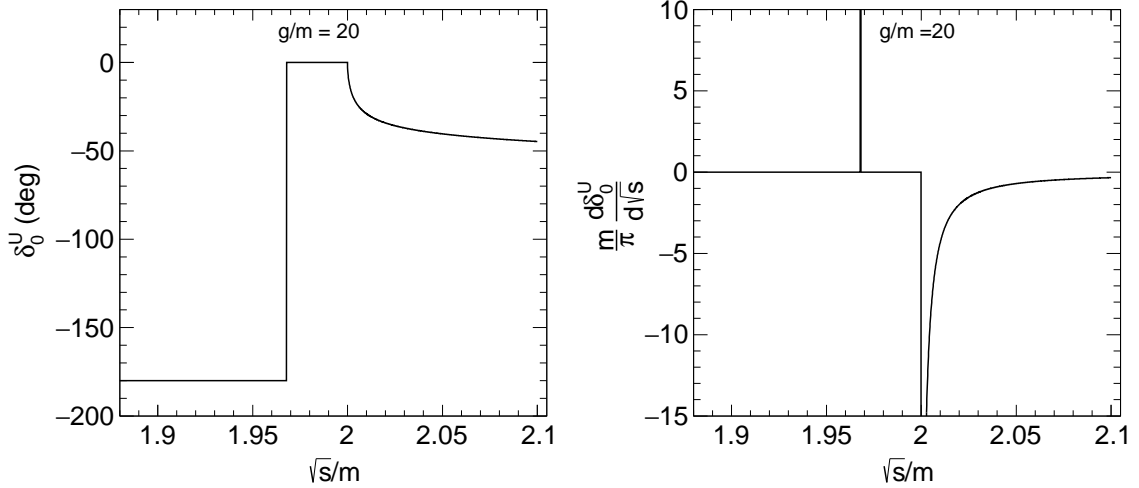


FIG. 5. (Left) Energy dependence of the s-wave phase-shift at $g = 20m > g_c$ below and above the threshold. One may note the jump from $-\pi/2$ at the bound state mass M_B . (Right) Corresponding energy dependence of the derivative of the phase shift. At $\sqrt{s} = M_B$ a Dirac-delta function appears.

is a sudden jump of the phase shift from $-\pi/2$ to zero (set as the conventional value at threshold). As a consequence, there is a delta function in the derivative of the phase shift shown in the right panel of Fig. 5 .

Note, Fig. 5 is consistent with the Levinson theorem [47, 48], according to which the number of poles below threshold equals to the difference of the phase shift at infinity and at threshold:

$$n_{\text{poles-below-threshold}} = \frac{1}{\pi} \left(\delta_0^U(s \rightarrow \infty) - \delta_0^U(s = 4m^2) \right) . \quad (36)$$

III. THERMODYNAMIC PROPERTIES OF THE φ^3 -QFT

In this section, we study the φ^3 -theory at nonzero temperature. In particular, we shall concentrate on the evaluation of the different contributions to the pressure.

A. Nonzero- T formalism

The non-interacting part of the pressure for a gas of interacting particles with mass m reads:

$$P_{\varphi,\text{free}} = -T \int_k \ln \left[1 - e^{-\beta\sqrt{k^2+m^2}} \right], \quad (37)$$

where $\int_k \equiv \int d^3k/(2\pi)^3$ and $\beta = 1/T$. In the scattering-matrix or the S -matrix formalism [37–39, 41, 49–53], the interacting part of the pressure is related to the derivative of the phase shift with respect to the energy by the following relation:

$$P_{\varphi\varphi\text{-int}}^U = -T \int_{2m}^{\infty} dx \frac{2l+1}{\pi} \sum_{l=0}^{\infty} \frac{d\delta_l^U(s=x^2)}{dx} \int_k \ln \left[1 - e^{-\beta\sqrt{k^2+x^2}} \right] = \sum_{l=0}^{\infty} P_{\varphi\varphi\text{-int},l}^U, \quad (38)$$

where $x = \sqrt{s}$.

Above the critical value $g = g_c$, a bound state is formed. The pressure corresponding to the bound state of mass M_B can be written as

$$P_B = -\theta(g_c - g)T \int_k \ln \left[1 - e^{-\beta\sqrt{k^2+M_B^2}} \right], \quad (39)$$

where the theta function takes into account that for $g < g_c$ there is no bound state B .

The total pressure of the system is written as

$$P_{\text{tot}}^U = P_{\varphi,\text{free}} + P_{\varphi\varphi\text{-int}} + P_B. \quad (40)$$

Quite interestingly, as discussed in Ref. [32], the bound-state and the interaction part can be summarized by the equation

$$P_{\varphi\varphi\text{-int}}^U + P_B = -T \int_0^{\infty} dx \frac{2l+1}{\pi} \sum_{l=0}^{\infty} \frac{d\delta_l^U(s=x^2)}{dx} \int_k \ln \left[1 - e^{-\beta\sqrt{k^2+x^2}} \right], \quad (41)$$

where the lowest range of the integral is set to zero. In this way, the bound state and the interaction part are taken into account by a unique expression that contains the derivative of the phase-shift(s) below the threshold. In other words, the bound state can be also understood as a manifestation of the interaction among the φ particles.

As a final remark, we stress that the equations presented above shall be valid for all the QFT examples that we are going to investigate.

B. Numerical results

Next, we turn to numerical examples and plots that allow showing the properties of the system at nonzero temperature.

Figure 6 shows the unitarized pressure ($P_{\varphi\varphi\text{-int},l}^U/T^4$) as a function of g/m at $T/m = 1$ for the partial waves corresponding $l = 0, 2, 4$. The s-wave is interesting: up to $g = g_c \approx 14.45$, $P_{\varphi\varphi\text{-int},l}^U/T^4$ increases, then it abruptly jumps to negative values. The reason is that above g_c a bound state exists.

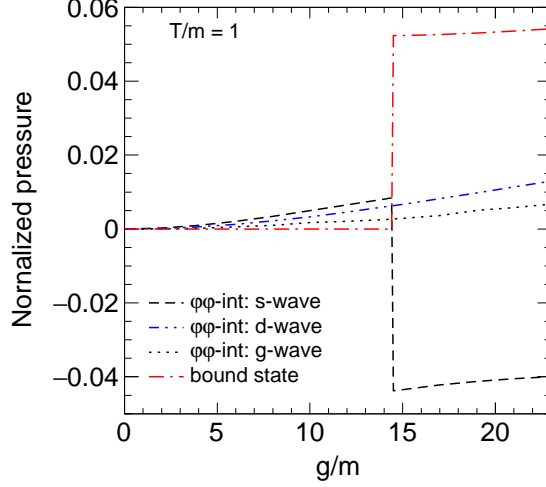


FIG. 6. Normalized interacting pressure ($P_{\varphi\varphi\text{-int},l}^U/T^4$ of Eq. 38) as function of g/m for three different partial waves corresponding to $l = 0$ (s-wave), $l = 2$ (d-wave) and $l = 4$ (g-wave) at $T/m = 1$. The normalized pressure for bound state (Eq. 39) is also shown.

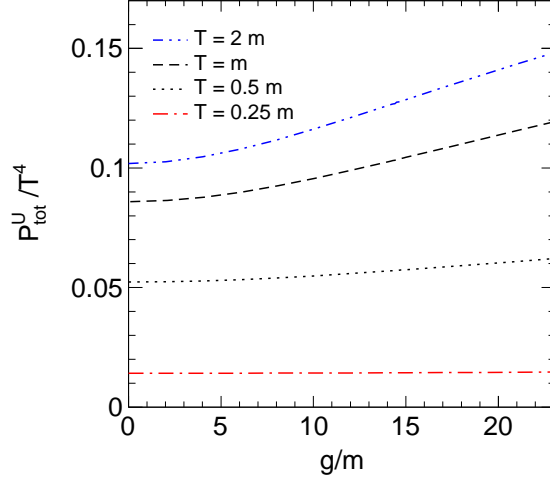


FIG. 7. Normalized total pressure (Eq. 40) as function of g/m at fixed T/m .

The normalized pressure (P_B/T^4) for the bound state (see Eq. 39) is also shown: it is zero below g_c and nonzero (and positive) above this value. The jump has the same magnitude but opposite sign of the s-wave interacting channel. Moreover, the variation of the normalized total pressure with g/m as evaluated via Eq. 40 is shown in Fig. 7. The normalized total pressure varies continuously with g in all four temperatures shown in this figure.

Next, Fig. 8 shows the interacting parts of the normalized pressure for the s-, d- and g-waves as a function of T/m for $g = 10m < g_c$ (no bound state). All the contributions are positive. We observe that at low T the s-wave dominates over the d- and g-waves. However, with the increase of T , the d- and g-waves become larger due to their larger degeneracy factors (5 and 9, respectively).

Figure 9 is similar to Fig. 8 but for $g = 20m > g_c$ (for which the bound state forms). The s-wave contribution is negative and decreasing, signaling a repulsion. Here, also the bound state contribution is plotted.

The total normalized pressure as a function of T/m is shown in Fig. 10 for three different values

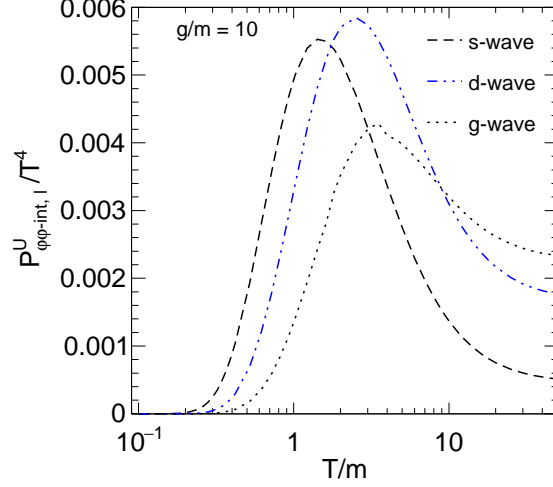


FIG. 8. Temperature dependence of the interacting normalized pressure (see Eq. 38) for s-, d- and g-waves at $g = 10m < g_c$.

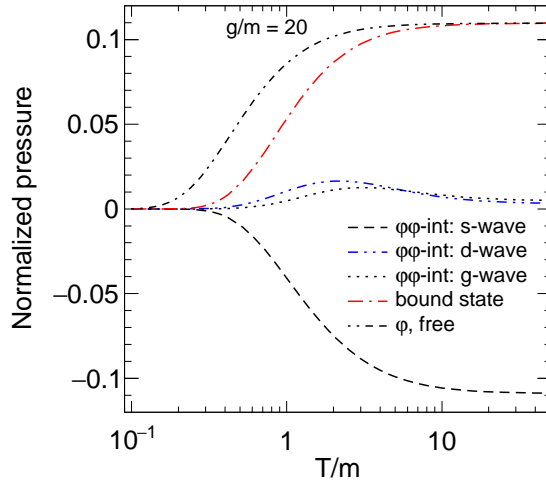


FIG. 9. Temperature dependence of the interacting normalized pressure (see Eq. 38) for s-, d- and g-waves at $g = 20m > g_c$ (bound state forms). Besides the interactions of s-, d- and g-waves, the normalized pressure of the bound state and of free particles are also shown.

of g (the free case $g = 0$, $g/m = 10$ and $g/m = 20$). At high T the massless limit $(P_{\varphi, \text{free}}/T^4)_{m=0} = \pi^2/90 \approx 0.1096$ is reached.

An important point concerns the quantification of the contribution of the interaction to the pressure. We discuss the scenarios without and with the bound state separately.

When no bound state forms ($g < g_c$), it is useful to define the quantity:

$$\eta = \frac{P_{\text{tot}}^U}{P_{\varphi, \text{free}}^U} = 1 + \frac{P_{\varphi\varphi\text{-int}}^U}{P_{\varphi, \text{free}}^U}. \quad (42)$$

The absence of interactions ($g \rightarrow 0$) corresponds to $\eta = 1$ and departures from this value quantify the naive result that one obtains by neglecting them.

Figure 11 shows the temperature dependence of η for two different values of $g < g_c$. For both cases $\eta \approx 1$ when T is low. This indicates that the role of the interaction is negligible at low temperatures.

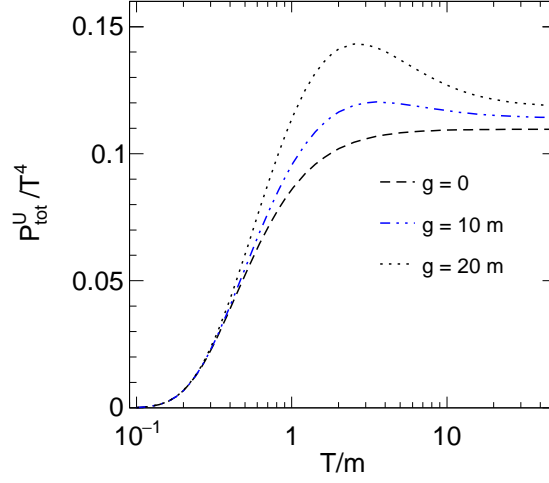


FIG. 10. Temperature dependence of the normalized total pressure (Eq. 40).

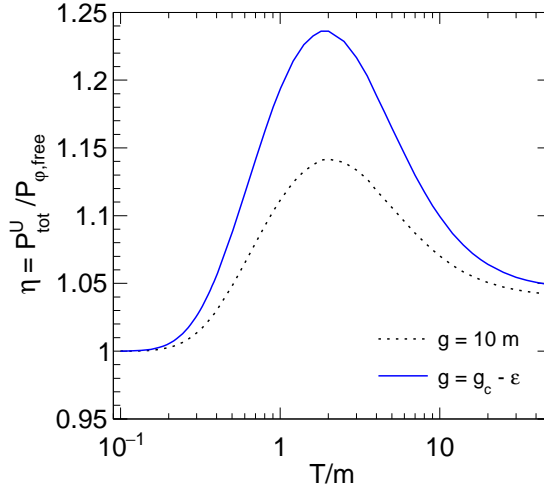


FIG. 11. Temperature dependence of the ratio η (Eq. 42).

With the increase of T/m , η increases and becomes maximal at around $T/m \approx 2$. Then, above this value, it decreases and saturates. Moreover, we notice that for $g = g_c - \epsilon$ the maximum is reached for $\eta \approx 1.23$, which indicates that the effect of interaction is non-negligible at certain intermediate temperatures. The height at the maximum decreases -as expected- with the decrease of g , since the interaction is less intense.

Let us now define an analogous quantity to be used when a bound state forms ($g > g_c$):

$$\zeta = \frac{P_{\varphi\varphi\text{-int}}^U + P_B}{P_B}, \quad (43)$$

out of which the total pressure of the system is given by

$$P_{\text{tot}}^U = P_{\varphi,\text{free}} + \zeta P_B, \quad (44)$$

which is simply the sum of two free gases, one for the particles of the type φ with mass m and one for the bound state B with mass M_B . Yet, the latter is rescaled by the factor ζ , which quantifies

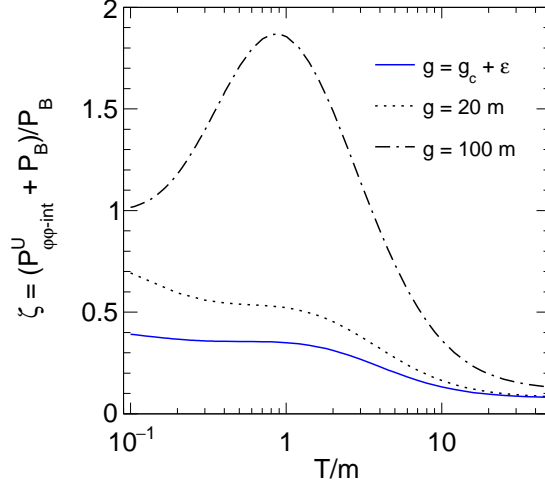


FIG. 12. Temperature dependence of the ratio ζ (Eq. 43).

the departure from the naive result obtained by including only a simple thermal contribution of free particles with mass M_B . Note, the naive case corresponds to $\zeta = 1$. In particular, the ratio ζ tells us how much of the bound state contribution remains after the partial cancellation induced by the interaction has been taken into account.

In Fig. 12 we show the temperature dependence of ζ for the values $g = g_c + \varepsilon$, $g = 20m$, and $g = 100m$. For $g = g_c + \varepsilon$, the quantity $\zeta \approx 0.4$ at $T/m = 0.1$, which then decreases for increasing T/m and saturates to ≈ 0.08 . For $g = 20m$, $\zeta \approx 0.7$ at low T/m and decreases to ≈ 0.08 at high T/m . Thus, in both cases, the joint role of the bound state and interaction can be summarized by a contribution of free gas of bound state particles which is sizably reduced by ζ . A partial cancellation takes place. Moreover, the amount of reduction depends both on the value of g as the value of temperature, being typically larger at small T and smaller at large T . In general, there is not a unique simple answer to the question about the amount of cancellation between the bound state gas and the interaction contributions.

Finally, the case $g = 100m$ can be regarded as a strong-coupling limit. Here, $\zeta > 1$, shows that one has even a larger result than a simple free gas of B particles. A closer inspection indicates that for large g the role of the d- and g-waves is sizable and the additional pressure is due to the higher waves.

C. Adding a four-leg interaction

As the last subject of this section, we show how the results change when adding an interaction term proportional to φ^4 . To this end, let us consider the Lagrangian

$$\mathcal{L} = \frac{1}{2} (\partial_\mu \varphi)^2 - \frac{1}{2} m^2 \varphi^2 - \frac{g}{3!} \varphi^3 - \frac{\lambda}{4!} \varphi^4, \quad (45)$$

whose tree-level scattering amplitude reads

$$A(s, t, u) = -\lambda - \frac{g^2}{s - m^2 + i\epsilon} - \frac{g^2}{t - m^2 + i\epsilon} - \frac{g^2}{u - m^2 + i\epsilon}. \quad (46)$$

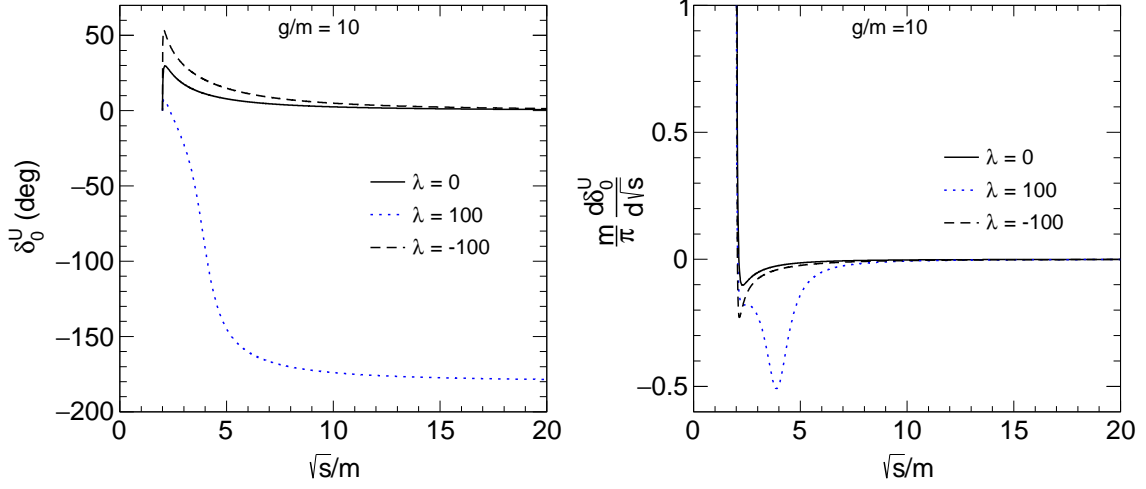


FIG. 13. (Left) Variation of the s-wave phase shift (using Eqs. 47 and 29) w.r.t. \sqrt{s}/m at $g = 10m$ when the additional φ^4 -term is present. (Right) Variation of the corresponding derivatives with respect to \sqrt{s}/m .

Only the s-wave amplitude is modified by including the φ^4 term, hence we shall concentrate only on the lowest wave in the following. The new expression for the tree-level s-wave amplitude reads:

$$A_0(s) = \frac{1}{2} \int_{-1}^{+1} d\xi A(s, \theta) = -\lambda - \frac{g^2}{s - m^2} + 2g^2 \frac{\log \left[1 + \frac{s - 4m^2}{m^2} \right]}{s - 4m^2}, \quad (47)$$

out of which the tree-level scattering length takes the form:

$$a_0^{\text{SL}} = \frac{1}{2} \frac{A_0(s = 4m^2)}{8\pi\sqrt{4m^2}} = \frac{-\lambda}{32\pi m} + \frac{1}{32\pi m} \frac{5g^2}{3m^2}. \quad (48)$$

The loop function allows calculating the unitarized amplitudes in the s -channel as:

$$A_0^U(s) = [A_0^{-1}(s) - \Sigma(s)]^{-1}, \quad (49)$$

where $\Sigma(s)$ is the loop function reported in Eq. (24), see also Ref. [46]. The unitarized scattering length reads:

$$a_0^{U,\text{SL}} = a_0^U(s = 4m^2) = \frac{1}{2} \frac{1}{16\pi m} \frac{1}{A_0^{-1}(4m^2) - \Sigma(4m^2)} \quad (50)$$

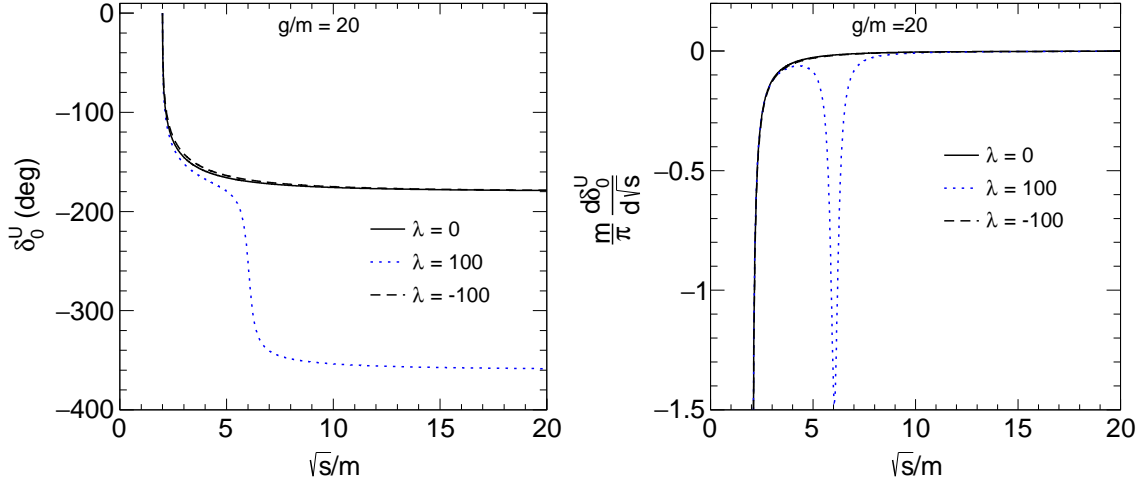
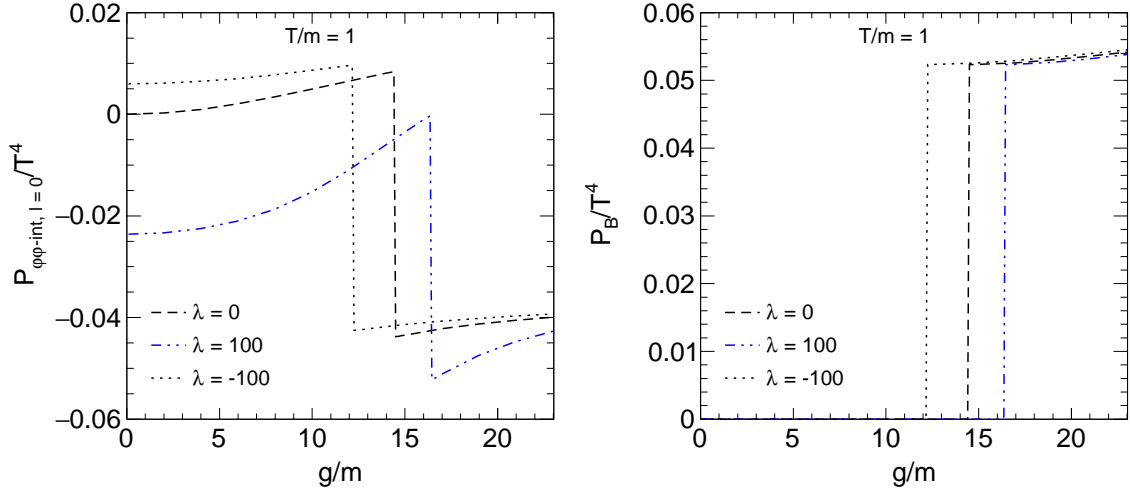
$$= \frac{1}{32\pi m} \frac{1}{\left[-\lambda + \frac{5g^2}{3m^2} \right]^{-1} - \frac{1}{64\sqrt{3}\pi}}. \quad (51)$$

For a certain fixed value of λ , the new critical value of g is given by

$$-\lambda + \frac{5g^2}{3m^2} = 64\sqrt{3}\pi,$$

then:

$$g_{\lambda,c}^2 = g_c^2 + \frac{3m^2}{5}\lambda \quad (52)$$

FIG. 14. Same as Fig. 13 but for $g = 20m$.FIG. 15. Variation of the normalized s-wave contribution to the pressure (left) (Eq. 38) and bound state (right) (Eq. 39) with g/m when the additional φ^4 -term is present.

In the left panel of Fig. 13 we show the s-wave phase shift as a function of \sqrt{s}/m for $g/m = 10$ and for three different values of λ ($\lambda = 0$ as reference, $\lambda = 100$ (repulsive) for which $g_{\lambda,c}/m \approx 16.4$, and $\lambda = -100$ (attractive) for which $g_{\lambda,c}/m \approx 12.2$, thus no bound state forms in any of these cases). Interestingly, the case $\lambda = -100$ is similar to $\lambda = 0$. Yet, the situation is completely different for $\lambda = 100$, where the phase shift decreases and saturates to $-\pi$ at large energies. Note, this result is not in disagreement with Levinson's theorem. Even if no physical pole is realized, there is a pole for negative s values which causes the phase shift to tend to $-\pi$, see also Ref. [32] where this feature is discussed for the φ^4 -theory. [indeed, this result is expected since for large energies the φ^4 -term dominates]. Finally, the phase-shift derivatives are shown in the right panel of Fig. 13.

Figure 14 is obtained for $g = 20m > g_{\lambda,c}$, for which a bound state forms. Correspondingly, the phase shift tends to $-\pi$ for high energies. Also here, the case $\lambda = -100$ is similar to $\lambda = 0$. A quite different behaviour is observed in the case of $\lambda = 100$ where at large \sqrt{s}/m the phase shift saturates to -2π , in agreement with the presence of two poles below threshold (one of which is the physical bound state). Note that the mass of the bound state is different for different λ values. For $\lambda = 0, 100$ and

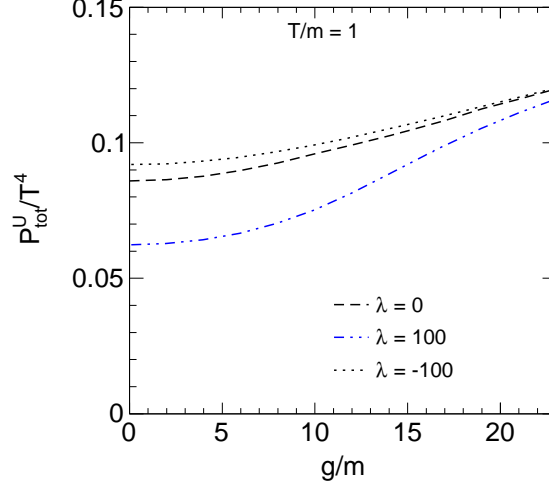


FIG. 16. Variation of the normalized total pressure (Eq. 40) with g/m when both the additional φ^4 -term is present.

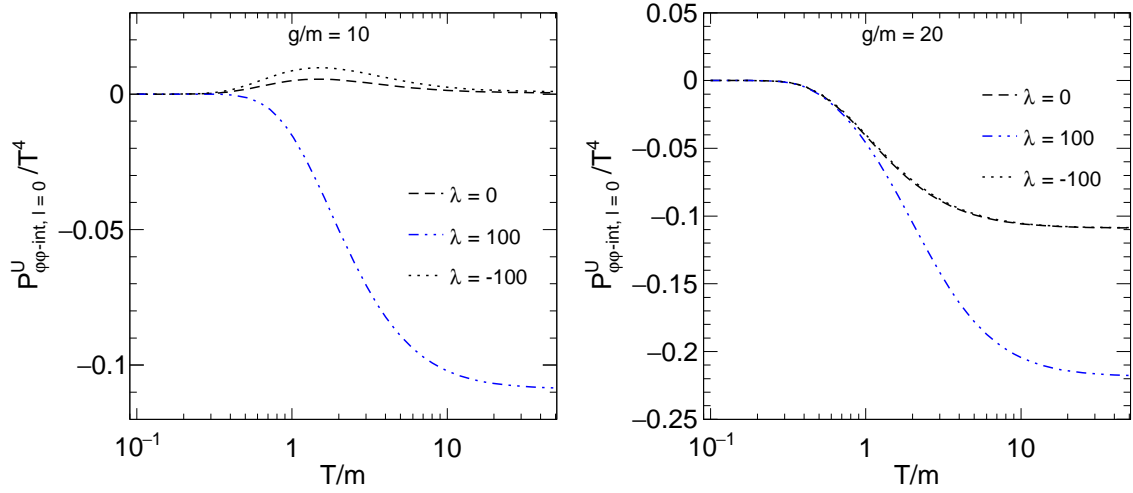


FIG. 17. Temperature dependence of the s-wave normalized pressure (Eq. 38) at different λ . The left panel is for $g = 10m < g_c$ (no bound state) and the right panel for $g = 20m > g_c$ (bound state builds).

-100, bound state masses are respectively $1.968m$, $1.98m$ and $1.955m$. The phase-shift derivatives are plotted in the right panel. Interestingly, a deep near $\sqrt{s}/m = 6$ is observed for $\lambda = 100$.

Next, we turn to the pressure. In the left panel of Fig. 15 we show the normalized s-wave interacting pressure as a function of g/m for three values of λ and for $T/m = 1$. Note, the discontinuity in the s-wave pressure corresponds to $g_{\lambda,c}$: the larger λ , the larger $g_{\lambda,c}$ needed to form a bound state, see Eq. (52). The normalized pressure of the bound state is shown in the right panel of Fig. 15, which -just as before- starts abruptly at $g_{\lambda,c}$. The total pressure is, as expected, continuous in g , see Fig. 16.

In Fig. 17 we show the temperature dependence of the s-wave normalized pressure for different λ (left panel for $g = 10m$ (no bound state), right panel for $g = 20m$ (bound state present)). For $g = 10m$, the s-wave contribution to the pressure is positive for $\lambda = 0$ and $\lambda = -100$, but is negative for $\lambda = 100$. On the other hand, for $g = 20m$ the s-wave pressure is negative for all the three λ 's.

The temperature dependence of total normalized pressure for $g = 10m$ and $20m$ are shown in Fig. 18. Note, for $\lambda = 100$ total pressure is significantly reduced w.r.t. the case $\lambda = 0$.

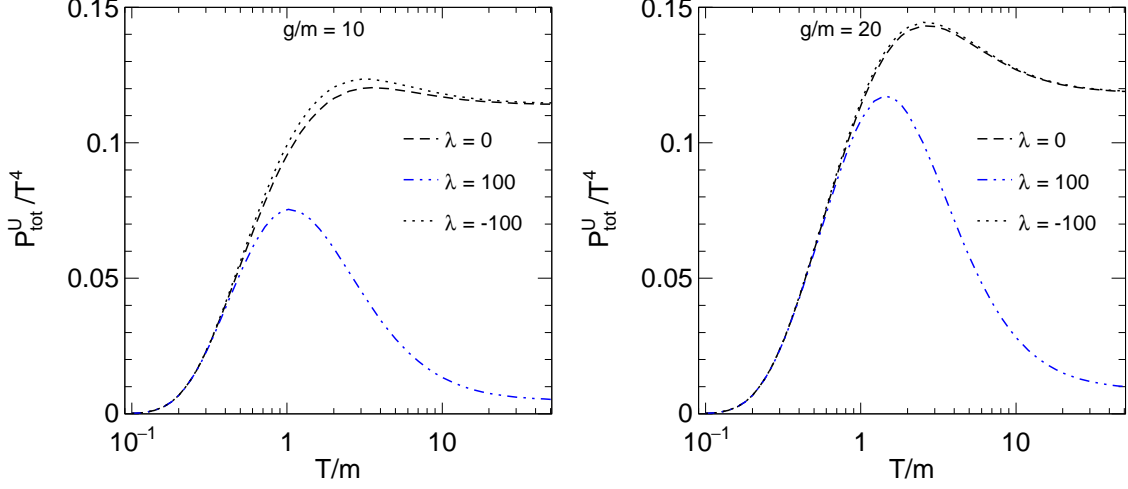


FIG. 18. (Left) Variation of the normalized total pressure (Eq. 40) with T/m at different λ . Left panel is obtained for $g = 10m$ and the right panel for $g = 20m$.

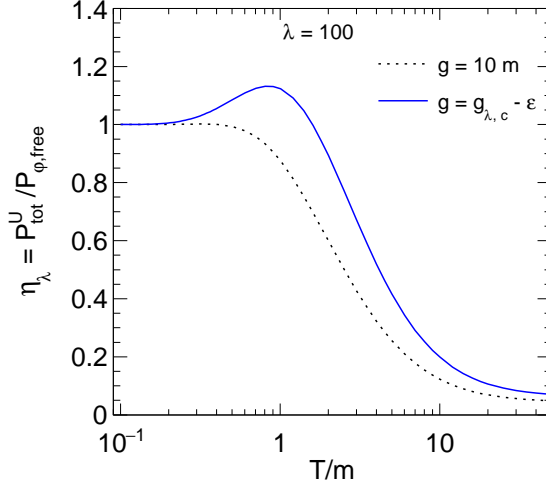


FIG. 19. Temperature dependence of the ratio η_λ for $\lambda = 100$ (Eq. 53).

In presence of the φ^4 interaction we define quantities similar to Eqs. 42 and 43 as follows:

$$\eta_\lambda = \frac{P_{\text{tot}}^U}{P_{\varphi,\text{free}}}, \quad (53)$$

$$\zeta_\lambda = \frac{P_{\varphi\varphi\text{-int}}^U + P_B}{P_B}. \quad (54)$$

These ratios are used to quantify the effect of the interaction. Figure 19 shows the variation of η_λ with T/m at $\lambda = 100$. Here we take two g values below the $g_{\lambda,c} \approx 16.4m$. For both cases, η_λ is very close to one at low and at large T/m , while a peak for $T/m \sim 1$ is realized.

In Fig. 20 we show temperature dependence ζ_λ for $\lambda = 100$ at $g = g_{\lambda,c} + \epsilon$ ($g_{\lambda,c} \approx 16.4m$), $g = 20m$ and $g = 100m$. Again, a partial cancellation of the single bound-state contribution is visible for $g = g_{\lambda,c} + \epsilon$ and $g = 20m$. For the strong coupling limit one observes also a ratio larger than one for intermediate temperatures.

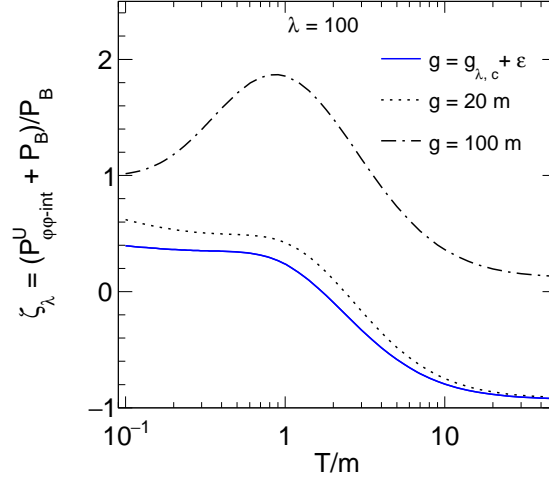


FIG. 20. Temperature dependence of the ratio ζ_λ for $\lambda = 100$ (Eq. 54).

IV. AN INTERMEDIATE STATE S

In this section, we study the case in which two distinct particles, φ with mass m and S with mass M , are considered. Their interaction is a three-leg $gS\varphi^2$ vertex. Thus, the decay of S into $\varphi\varphi$, if kinematically allowed, takes place. Then, the state S is a resonance with a certain decay width. Since two φ particles interact via an exchange of S , and attracting Yukawa-interaction between them is induced: if it is strong enough, a bound-state forms. The main question here is how this system behaves at nonzero T .

A. Vacuum's formalism

The Lagrangian under study takes the form:

$$\mathcal{L} = \frac{1}{2} (\partial_\mu \varphi)^2 - \frac{1}{2} m^2 \varphi^2 + \frac{1}{2} (\partial_\mu S)^2 - \frac{1}{2} M^2 S^2 + \frac{g}{2!} S \varphi^2, \quad (55)$$

where g is the coupling constant. The tree-level decay width $S \rightarrow \varphi\varphi$ (allowed for $M > 2m$) reads (e.g. Ref. [33]):

$$\Gamma_S = \frac{g^2}{2} \frac{\sqrt{\frac{M^2}{4} - m^2}}{8\pi M^2}, \quad (56)$$

and the tree-level scattering is:

$$A(s, t, u) = \frac{-g^2}{s - M^2 + i\epsilon} + \frac{-g^2}{t - M^2 + i\epsilon} + \frac{-g^2}{u - M^2 + i\epsilon}. \quad (57)$$

The first three tree-level partial wave amplitudes are evaluated as:

$$A_0(s) = \frac{1}{2} \int_{-1}^{+1} d\xi A(s, \theta) = -\frac{g^2}{s - M^2 + i\epsilon} + 2g^2 \frac{\log \left[1 + \frac{s - 4m^2}{M^2} \right]}{s - 4m^2 + i\epsilon}; \quad (58)$$

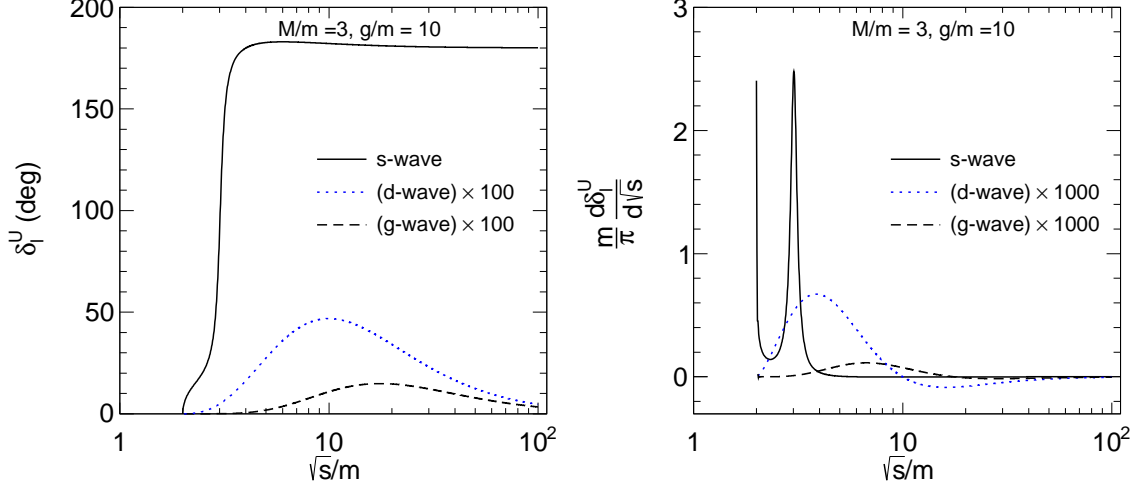


FIG. 21. (Left) Variation of phase shifts with \sqrt{s}/m for s -, d -, and g -waves at $g = 10m < g_{S,c}$ when the resonance S has mass $M = 3m$. The d - and g -wave phase shifts are multiplied by a factor of 100 to make them visible. (Right) Energy dependence of s -, d -, g -wave phase-shift derivatives. The d - and g -waves contributions are multiplied by a factor of 1000.

$$A_2(s) = \frac{-2g^2}{(s - 4m^2)^3} (3(4m^2 - s)(4m^2 - 2M^2 - s) + (16m^4 + 6M^4 + 6M^2s + s^2 - 8m^2(3m^2 + s)) \log \left[1 + \frac{s - 4m^2}{M^2} \right]); \quad (59)$$

$$A_4(s) = \frac{-2g^2}{3(s - 4m^2)^3} [5(4m^2 - s)(4m^2 - 2M^2 - s)(80m^4 - 8m^2(21M^2 + 5s) + 42M^4 + 42M^2s + 5s^2) - 6(256m^8 - 256m^6(5M^2 + s) + 96m^4(15M^4 + 10M^2s + s^2) - 16m^2(35M^6 + 45M^4s + 15M^2s^2 + s^3) + 70M^8 + 140M^6s + 90M^4s^2 + 20M^2s^3 + s^4) \log(1 + \frac{s - 4m^2}{M^2})]. \quad (60)$$

The unitarization is carried out by repeating analogous steps as in Sec. II B. As previously, the loop function for $M < 2m$ (when the state S is stable) has therefore two subtractions, one at the mass M and one at the branch point $4m^2 - M^2$:

$$\Sigma(s) = -\frac{(s - M^2)(s - (4m^2 - M^2))}{\pi} \int_{4m^2}^{\infty} \frac{\frac{1}{2} \frac{\sqrt{\frac{s'}{4} - m^2}}{8\pi\sqrt{s'}}}{(s - s' + i\varepsilon)(s' - M^2)(s' - (4m^2 - M^2))} ds'. \quad (61)$$

Yet, for $M > 2m$ (that is above threshold) the state S is a resonance, therefore we should only require that the real part of the loop vanishes at M^2 , thus $\text{Re}[\Sigma(s = M^2)] = 0$ (the whole loop does not, since the imaginary part, proportional to the decay width of S , is nonzero). Then:

$$\Sigma(s) = \Sigma(s) = -\frac{(s - (4m^2 - M^2))}{\pi} \int_{4m^2}^{\infty} \frac{\frac{1}{2} \frac{\sqrt{\frac{s'}{4} - m^2}}{8\pi\sqrt{s'}}}{(s - s' + i\varepsilon)(s' - (4m^2 - M^2))} ds' + C, \quad (62)$$

where the subtraction C is such that $\text{Re}[\Sigma(s = M^2)] = 0$.

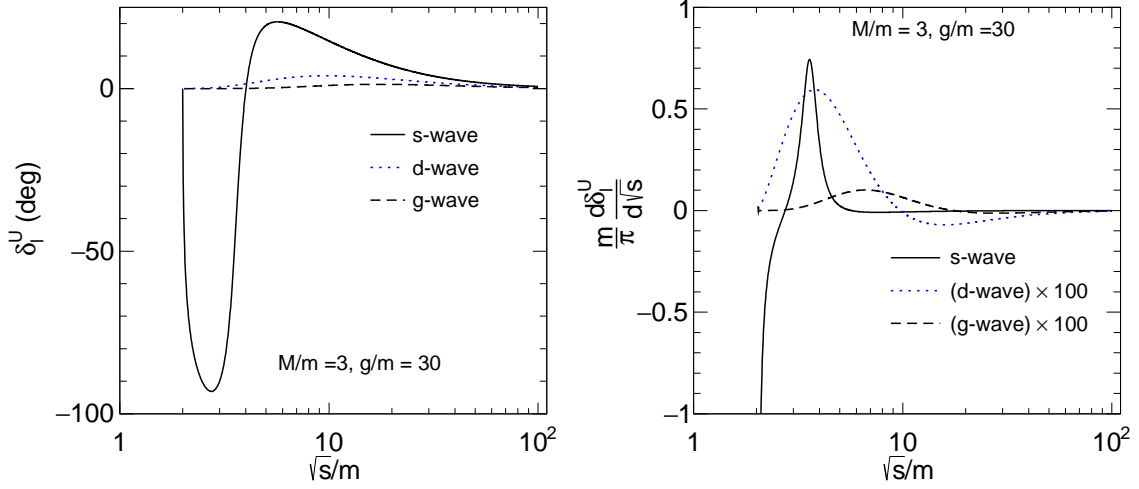


FIG. 22. Similar to Fig. 21 but for $g = 30m > g_{S,c}$. The d- and g-wave phase shift derivatives are multiplied by a factor of 100.

The unitarized amplitudes are given by $A_k^U(s) = [A_k^{-1}(s) - \Sigma(s)]^{-1}$, thus the critical value of the coupling g for obtaining a bound state in the s-channel is determined by

$$A_0^{-1}(4m^2) - \Sigma(4m^2) = 0 \quad (63)$$

with

$$A_0(s = 4m^2) = \frac{-g^2}{4m^2 - M^2} + \frac{2g^2}{M^2}; \quad (64)$$

$$\Sigma(4m^2) = \frac{\sqrt{M^2 - 4m^2} \log \left[-1 + \frac{M(M + \sqrt{M^2 - 4m^2})}{2m^2} \right]}{32M\pi^2}. \quad (65)$$

Note, the fact that a critical g is needed to obtain a bound state is well known in the quantum mechanical counterpart of the Yukawa interaction, e.g. Refs. [54, 55].

The energy dependence of the unitarized phase shifts for s-, d- and g-waves is shown in the left panel of Fig. 21 for the choice $M = 3m$ and $g = 10m < g_{M,c} \approx 22.83m$. The s-wave phase increases rapidly near $\sqrt{s} = 3m = M$ and tends towards $\approx \pi$ (from above). Compared to the s-wave, magnitudes of the d- and g-wave phase shifts are significantly smaller and hence they are multiplied by a factor of 100 to show them in this plot.

The derivative of the corresponding phase shifts with respect to \sqrt{s}/m is shown in the right panel of Fig. 21. At the threshold, the derivative of s-wave phase shift is infinite (but the area under the curve is finite, hence there is no problem in evaluating thermodynamical quantities, see below). As expected, a resonance peak is observed near $\sqrt{s} = 3m = M$. The reason for this peak is the presence of the particle S of mass $3m$. For d- and g-waves, the derivatives of phase shifts are multiplied by a factor of 1000 to show them in the same plot since their magnitudes are smaller compared to that of s-wave.

In the left panel of Fig. 22 the case $g = 30m > g_{M,c}$ is shown. A drastic change in the s-wave phase shift is observed, which is negative for $2m < \sqrt{s} \lesssim 4m$, as a consequence of the presence of a bound state below the threshold. In this region, the s-wave phase shift decreases and reaches $-\pi/2$ around $\sqrt{s}/m \approx 3$, then starts increasing and becomes positive above $\sqrt{s}/m \approx 4$. It tends to zero at large \sqrt{s}/m . For the other two waves, the behaviour is similar to Fig. 21, but somewhat larger in magnitude. The right panel of Fig. 22 shows the derivatives of phase shifts. The derivative of the s-wave phase shift starts from $-\infty$ at the threshold, it then increases rapidly with the increase

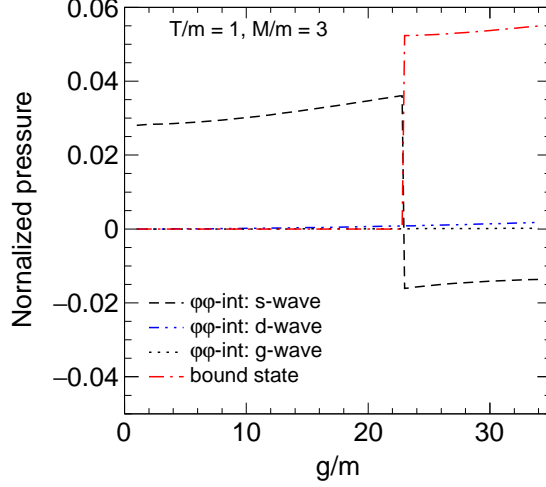


FIG. 23. Variation of normalized pressure of s-, d- and g-waves with g/m at fixed T/m in presence of an intermediate state S of mass $M = 3m$. The normalized pressure of the bound state is also shown.

of \sqrt{s}/m and becomes positive. Around $\sqrt{s}/m \approx 3.5$ it shows a peak and starts decreasing towards zero above that. The variation of derivatives of the d- and g-waves are similar Fig. 21, but larger in magnitude.

B. Thermodynamic properties of the system in presence of S

In this subsection, we discuss the thermodynamical properties of the system in presence of an intermediate state S with mass M . The pressure is evaluated via Eq. (38), that we report for convenience:

$$P_{\varphi\varphi\text{-int}}^U + P_B = -T \int_0^\infty dx \frac{2l+1}{\pi} \sum_{l=0}^\infty \frac{d\delta_l^U(s=x^2)}{dx} \int_k \ln \left[1 - e^{-\beta\sqrt{k^2+x^2}} \right], \quad (66)$$

which gives the overall interacting contribution. In particular, it should be stressed that:

- (i) The pressure of the bound state P_B is, as usual, nonzero only for $g > g_{M,c}$.
- (ii) The contribution of the state S is contained in the term $P_{\varphi\varphi\text{-int}}^U$; in the limit $g \rightarrow 0$, one has

$$\frac{1}{\pi} \frac{d\delta_0^U(s=x^2)}{dx} = \delta(x-M), \quad (67)$$

thus $P_{\varphi\varphi\text{-int}}^U$ reduces to the pressure of free S particles with mass M .

(iii) Care is needed when $g = 0$. For this choice, the interaction contribution is, clearly, exactly zero. The state S is a free field that *cannot* be obtained from the interaction part of the φ field. This issue is discussed in details in Ref. [39]: Eq. (66) is valid for nonzero (even if infinitesimal) g :

$$\lim_{g \rightarrow 0} P_{\varphi\varphi\text{-int}}^U = P_{S,\text{free}} \neq (P_{\varphi\varphi\text{-int}}^U)_{g=0} = 0. \quad (68)$$

Next, we turn to numerical examples for the specific choice $M = 3m$. The interacting part of the normalized pressure of s-, d- and g-waves as a function of g/m is shown in Fig. 23, in which the temperature is taken as $T = m$. When g/m is small, the interacting part of the pressure of the s-wave is dominated by the free particle S with mass $M = 3m$. As the coupling g increases, the interacting part of the pressure of the s-wave contribution also increases. Up to the critical value of $g_{M,c} (\approx 22.83m)$,

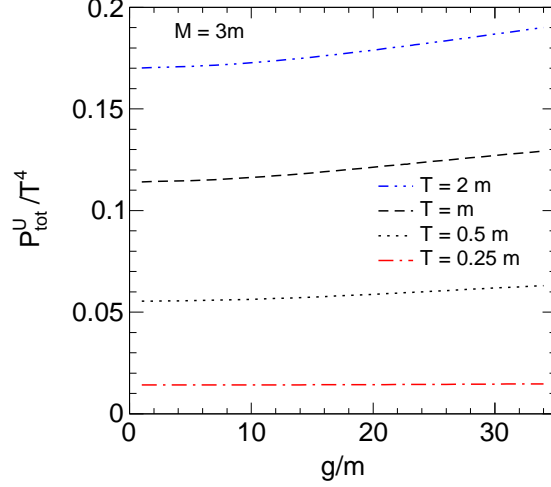


FIG. 24. Variation of the normalized total pressure (Eq. 40) with g/m in presence of an intermediate state of mass $M = 3m$.

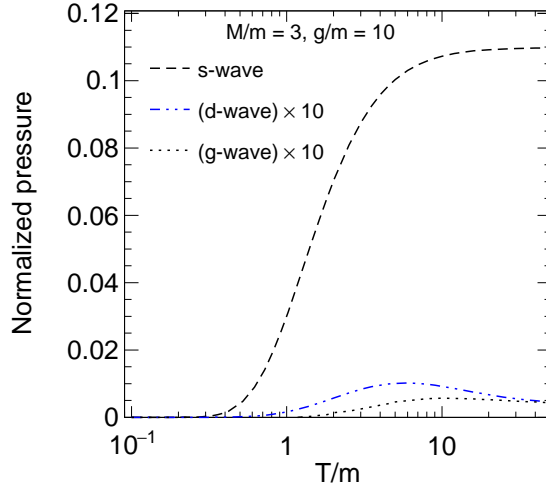


FIG. 25. Temperature dependence of the normalized pressure for s-, g-, and d-wave at $g = 10m < g_{S,c}$ in presence of an intermediate state S of mass $M = 3m$. Results of d- and g-waves are multiplied by a factor of 10.

the s-wave has a positive contribution to the pressure, while it is negative above it. The interacting part of the normalized pressure of d- and g-waves are always positive, but the magnitudes are much smaller compared to that of the s-wave. In this plot, we also show the normalized pressure for the bound state (which is clearly nonzero only for $g > g_{M,c}$). As in the previous QFT examples, the pressure of the bound state exactly compensates for the abrupt jump in the s-wave pressure at the critical value $g_{M,c}$. The normalized total pressure as a function of g/m for four different T is shown in Fig. 24. Similar to Figs. 7 and 16, the total pressure is continuous in g .

Next, we calculate the temperature dependence of the pressure for s-, d- and g-waves in presence of an intermediate state S of mass $M = 3m$. In Fig. 25 we show the results for $g/m = 10$. (The d- and g-waves contributions are multiplied by 10 to make them visible). For all three waves, the normalized pressure increases and saturates at large T/m .

Figure 26 shows the case $g = 30m > g_{M,c}$, for which a bound state forms. The pressure of the bound

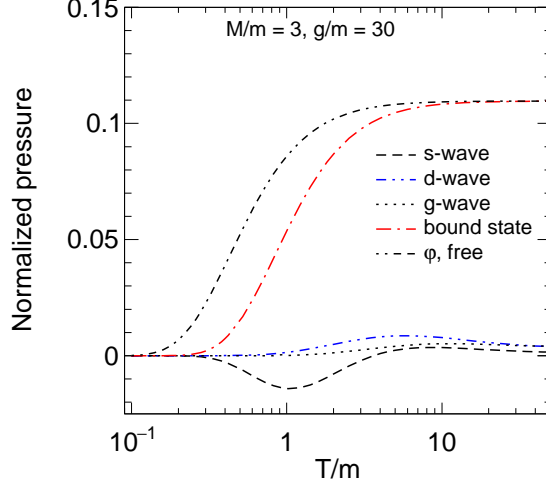


FIG. 26. Similar to Fig. 25 but for $g = 30m > g_{S,c}$. The pressure of bound state and free particles φ are also shown.

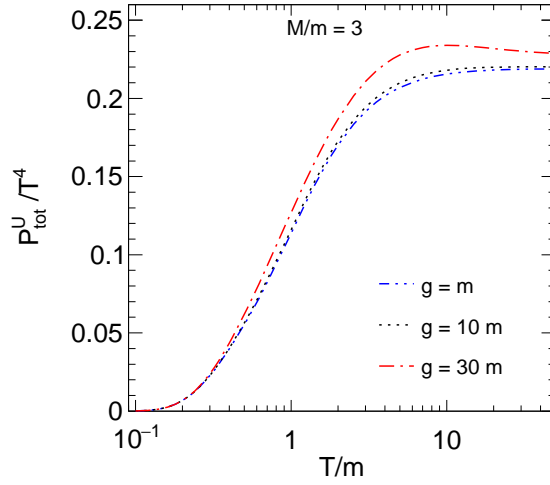


FIG. 27. Variation of normalized total pressure (Eq. 40) with temperature in presence of an intermediate state of mass $M = 3m$.

state, as well as free particle φ , are also shown. Both of them saturate at the value $\pi^2/90 \approx 0.109$ at high T/m . The normalized pressure for the s-wave is negative up to $T/m \approx 3.5$ and, beyond that, is slightly positive. The other two waves contribute positively. The magnitudes of three partial wave contributions are small compared to contributions of the free particles φ and the bound state B . The temperature dependence of the normalized total pressure as a function of T/m is shown for three values of g in Fig. 27.

When $g = m \ll g_{M,c}$, the attraction is very small and the resonance S behaves almost like a free particle, thus basically the two free particles φ and S contribute to the pressure. At large T the normalized pressure saturates to $2\pi^2/90 \approx 0.219$. For the larger coupling $g = 10m$, the state S has a sizable width. As a result, the normalized total pressure is larger than the one for $g = m$. For $g = 30m$, there is, in addition, also a bound state. Although the pressure of s-wave is negative up to certain T/m (see Fig. 26), the overall effect of the interaction for $g = 30m$ is, as expected, positive.

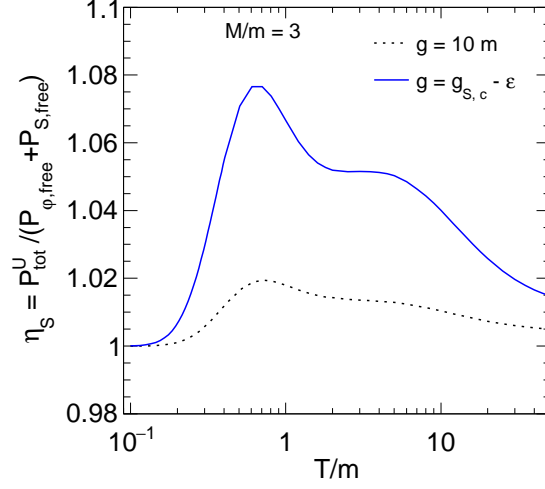


FIG. 28. Variation of the ratio η (Eq. 69) with temperature in presence of an intermediate state of mass $M = 3m$ (no bound state present).

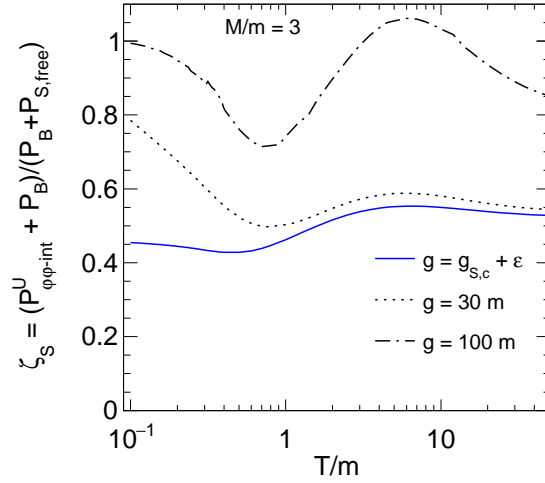


FIG. 29. Variation of the ratio ζ (Eq. 70) with temperature in presence of an intermediate state of mass $M = 3m$ (a bound state is present).

Finally, in order to study the overall effect of the interaction, we define the following ratios:

$$\eta_S = \frac{P_{\text{tot}}^U}{P_{\varphi,\text{free}} + P_{S,\text{free}}}, \quad (69)$$

and

$$\zeta_S = \frac{P_{\varphi\varphi\text{-int}} + P_B}{P_{S,\text{free}} + P_B}. \quad (70)$$

In Fig. 28 we show η_S as a function of T/m at two different g below the critical value $g_{M,c}$. For both cases, η_S is greater than one. This implies that neglecting interaction would lead to underestimation of the overall actual pressure.

In Fig. 29 we show ζ_S with T for three different g , one just above the critical value $g_{M,c} \approx 22.83m$ and for $g = 30m$ and $g = 100m$. For the first case, $\zeta_S \approx 1$ at low temperature but, as T/m increases, it decreases and reaches a minimum value ≈ 0.43 for $T/m \approx 0.5$. With further increase of T/m , the ratio ζ_S slightly increases and saturates at a value ≈ 0.52 . For $g = 30m$, the behaviour of ζ_S is qualitatively similar to the previous one, but at high T/m it saturates to ≈ 0.55 . In both cases, that neglecting the interaction would lead to a quite large overestimation of the actual result. Finally, for the strong coupling $g = 100m$, the ratio ζ_S is close to unity. Quite interestingly, the various effects compensate in such a way that the free gas with the resonance S and the bound state B reproduce quite well the interacting contribution to the pressure.

V. CONCLUSIONS

In this work, we have investigated the role of particle interaction in a thermal gas in the context of selected scalar QFTs that contain three-leg vertices and can lead to the formation of bound states, if the attraction is strong enough.

To this end, we have calculated the scattering phase shifts of the s-, d-, and g-waves using the partial wave decomposition of two-body scattering and we implemented a non-perturbative unitarized one-loop resummed approach for which the theory is unitary, finite and well defined for each value of the three-leg coupling constant g .

QFT	Quantity	Total pressure P_{tot}^U	Figure
$\frac{g}{3!}\varphi^3$	η	$P_{tot}^U = \eta P_{\varphi,free}$	11
$\frac{g}{3!}\varphi^3 + \frac{\lambda}{4!}\varphi^4$	η_λ	$P_{tot}^U = \eta_\lambda P_{\varphi,free}$	19
$\frac{g}{2!}S\varphi^2$	η_S	$P_{tot}^U = \eta_S (P_{\varphi,free} + P_{S,free})$ $= P_{\varphi,free} + \zeta_S P_{S,free}$	28

TABLE I. Estimate of the interaction's role when no bound state forms (g less than the respective critical values). In each case, the expected value in absence of the interaction is one.

QFT	Quantity	Total pressure P_{tot}^U	Figure
$\frac{g}{3!}\varphi^3$	ζ	$P_{tot}^U = P_{\varphi,free} + \zeta P_B$	12
$\frac{g}{3!}\varphi^3 + \frac{\lambda}{4!}\varphi^4$	ζ_λ	$P_{tot}^U = P_{\varphi,free} + \zeta_\lambda P_B$	20
$\frac{g}{2!}S\varphi^2$	ζ_S	$P_{tot}^U = P_{\varphi,free} + \zeta_S (P_{S,free} + P_B)$	29

TABLE II. Estimate of the interaction's role when a bound state forms (g greater than the respective critical values). In each case, the expected value in absence of the interaction is one.

In all cases, we studied the role of the interaction and realized that, in general, it is non-negligible. Even in the case when no bound state is present, a sizable role of the interaction implies that the simple inclusion of a gas of free φ particles maybe not be sufficient. In general, an attractive interaction (alias, a positive phase-shift derivative) implies an increase of pressure and vice-versa. This is understandable in a gas at zero chemical potential determined only by the vacuum's density of states (see below), but it should stress that this is quite different from the classical case, as e.g. the van der Waals gas, in which (at fixed number of particles) a repulsion induces an increase of the pressure, see also the discussion in Ref. [56].

Conversely, when a bound state forms, the simple inclusion of the bound state into the thermal gas is not enough for a correct description of the pressure of the system. Typically, a partial cancellation between the negative contribution of the interaction with the positive of the bound state occurs.

We summarize our results in Table I and Table II. In table, I, the cases in which the interaction does not lead to the formation of a bound state are presented, while in Table II the cases for which a bound state appears are listed. It is then clear that the answer to our original questions about the role of the interaction, as well as bound state and resonances, is not a simple one. The results depend on the coupling strength and eventually other parameters and on the temperature range. Yet, as a general statement, our results show that the role of the interaction can be sizable and the consideration of a simple free gas is in most cases insufficient.

In the end, we turn back to the original question formulated in the introduction about the quite peculiar production of a bound state at a nonzero temperature in thermal models, according to which the multiplicity depends solely on the mass of the bound state but is not affected by the typically large dimension of a composite object. In our approach, the phase-shift calculated in the vacuum is the quantity that is used to obtain the properties of the system at any temperature. Since the partition function $Z = \sum_n e^{-E_n/T}$ is determined by the energy eigenvalues E_n calculated in the vacuum, once these are known, the quantity Z is fixed for each temperature. In other words, Z is solely fixed by vacuum's physics. In our work, the sum over the states is replaced by an integral over the derivatives of the spectral function, but the basic idea is the same since the pressure is still determined by vacuum quantities. It is then quite natural within this context that the production is not related to the dimension of the composite objects. Yet, one may investigate this issue more in detail in the future. When a bound state is close to threshold forms, it can be understood via non-relativistic properties, see e.g. Ref. [57–59].

As an additional outlook, we mention the extension of the present work to particles with spins (both bosons and fermions), with particular attention to the direct study of nuclei as bound states of nucleons. The easiest of such systems is the deuteron.

Acknowledgments: The authors thank W. Broniowski and S. Mrowczynski for useful discussions about the thermodynamics of bound states and A. Pilloni for scattering issues. F.G. acknowledges financial support from the Polish National Science Centre NCN through the OPUS projects no. 2019/33/B/ST2/00613. S.S. acknowledges financial support from the Ulam Scholarship of the Polish National Agency for Academic Exchange (NAWA) with the agreement no: PPN/ULM/2019/1/00093/U/00001.

-
- [1] V. T. Cocconi, T. Fazzini, G. Fidecaro, M. Legros, N. H. Lipman, and A. W. Merrison, *Mass Analysis of the Secondary Particles Produced by the 25-GeV Proton Beam of the Cern Proton Synchrotron*, *Phys. Rev. Lett.* **5** (1960) 19–21.
 - [2] **STAR** Collaboration, B. I. Abelev et al., *Observation of an Antimatter Hypernucleus*, *Science* **328** (2010) 58–62, [[arXiv:1003.2030](#)].
 - [3] **STAR** Collaboration, H. Agakishiev et al., *Observation of the antimatter helium-4 nucleus*, *Nature* **473** (2011) 353, [[arXiv:1103.3312](#)]. [Erratum: *Nature*475,412(2011)].
 - [4] **ALICE** Collaboration, J. Adam et al., *Production of light nuclei and anti-nuclei in pp and Pb-Pb collisions at energies available at the CERN Large Hadron Collider*, *Phys. Rev.* **C93** (2016), no. 2 024917, [[arXiv:1506.08951](#)].
 - [5] **STAR** Collaboration, J. Adam et al., *Measurement of the mass difference and the binding energy of the hypertriton and antihypertriton*, *Nature Phys.* **16** (2020), no. 4 409–412, [[arXiv:1904.10520](#)].
 - [6] **ALICE** Collaboration, S. Acharya et al., *Production of (anti-)³He and (anti-)³H in p-Pb collisions at $\sqrt{s_{NN}} = 5.02$ TeV*, *Phys. Rev.* **C101** (2020), no. 4 044906, [[arXiv:1910.14401](#)].
 - [7] **ALICE** Collaboration, S. Acharya et al., *(Anti-)Deuteron production in pp collisions at $\sqrt{s} = 13$ TeV*, [arXiv:2003.03184](#).
 - [8] A. Esposito, A. L. Guerrieri, F. Piccinini, A. Pilloni, and A. D. Polosa, *Four-Quark Hadrons: an Updated Review*, *Int. J. Mod. Phys. A* **30** (2015) 1530002, [[arXiv:1411.5997](#)].
 - [9] **LHCb** Collaboration, R. Aaij et al., *Observation of a narrow pentaquark state, $P_c(4312)^+$, and of two-peak structure of the $P_c(4450)^+$* , *Phys. Rev. Lett.* **122** (2019), no. 22 222001, [[arXiv:1904.03947](#)].

- [10] P. J. Siemens and J. I. Kapusta, *Evidence for a soft nuclear matter equation of state*, *Phys. Rev. Lett.* **43** (1979) 1486–1489.
- [11] A. Andronic, P. Braun-Munzinger, J. Stachel, and H. Stocker, *Production of light nuclei, hypernuclei and their antiparticles in relativistic nuclear collisions*, *Phys. Lett.* **B697** (2011) 203–207, [arXiv:1010.2995].
- [12] A. Andronic, P. Braun-Munzinger, K. Redlich, and J. Stachel, *The statistical model in Pb-Pb collisions at the LHC*, *Nucl. Phys.* **A904-905** (2013) 535c–538c, [arXiv:1210.7724].
- [13] J. Cleymans, S. Kabana, I. Kraus, H. Oeschler, K. Redlich, and N. Sharma, *Antimatter production in proton-proton and heavy-ion collisions at ultrarelativistic energies*, *Phys. Rev.* **C84** (2011) 054916, [arXiv:1105.3719].
- [14] P. G. Ortega, D. R. Entem, F. Fernandez, and E. Ruiz Arriola, *Counting states and the Hadron Resonance Gas: Does $X(3872)$ count?*, *Phys. Lett.* **B781** (2018) 678–683, [arXiv:1707.01915].
- [15] P. G. Ortega and E. Ruiz Arriola, *Is $X(3872)$ a bound state?*, *Chin. Phys. C* **43** (2019), no. 12 124107, [arXiv:1907.01441].
- [16] S. T. Butler and C. A. Pearson, *Deuterons from High-Energy Proton Bombardment of Matter*, *Phys. Rev.* **129** (1963) 836–842.
- [17] A. Schwarzschild and C. Zupancic, *Production of Tritons, Deuterons, Nucleons, and Mesons by 30-GeV Protons on A-1, Be, and Fe Targets*, *Phys. Rev.* **129** (1963) 854–862.
- [18] H. H. Gutbrod, A. Sandoval, P. J. Johansen, A. M. Poskanzer, J. Gosset, W. G. Meyer, G. D. Westfall, and R. Stock, *Final State Interactions in the Production of Hydrogen and Helium Isotopes by Relativistic Heavy Ions on Uranium*, *Phys. Rev. Lett.* **37** (1976) 667–670.
- [19] H. Sato and K. Yazaki, *On the coalescence model for high-energy nuclear reactions*, *Phys. Lett.* **98B** (1981) 153–157.
- [20] S. Mrowczynski, *On the neutron proton correlations and deuteron production*, *Phys. Lett.* **B277** (1992) 43–48.
- [21] L. P. Csernai and J. I. Kapusta, *Entropy and Cluster Production in Nuclear Collisions*, *Phys. Rept.* **131** (1986) 223–318.
- [22] S. Mrowczynski, *Production of light nuclei in the thermal and coalescence models*, *Acta Phys. Polon.* **B48** (2017) 707, [arXiv:1607.02267].
- [23] S. Bazak and S. Mrowczynski, *^4He vs. ^4Li and production of light nuclei in relativistic heavy-ion collisions*, *Mod. Phys. Lett.* **A33** (2018), no. 25 1850142, [arXiv:1802.08212].
- [24] Z.-J. Dong, G. Chen, Q.-Y. Wang, Z.-L. She, Y.-L. Yan, F.-X. Liu, D.-M. Zhou, and B.-H. Sa, *Energy dependence of light (anti)nuclei and (anti)hypertriton production in the Au-Au collision from $\sqrt{s_{NN}} = 11.5$ to 5020 GeV*, *Eur. Phys. J.* **A54** (2018), no. 9 144, [arXiv:1803.01547].
- [25] K.-J. Sun and L.-W. Chen, *Production of $\Lambda\Lambda$ and $\bar{\Lambda}n$ in central Pb+Pb collisions at $\sqrt{s_{NN}} = 2.76$ TeV within a covariant coalescence model*, *Phys. Rev.* **C94** (2016), no. 6 064908, [arXiv:1607.04037].
- [26] K.-J. Sun, L.-W. Chen, C. M. Ko, J. Pu, and Z. Xu, *Light nuclei production as a probe of the QCD phase diagram*, *Phys. Lett.* **B781** (2018) 499–504, [arXiv:1801.09382].
- [27] A. Polleri, J. P. Bondorf, and I. N. Mishustin, *Effects of collective expansion on light cluster spectra in relativistic heavy ion collisions*, *Phys. Lett.* **B419** (1998) 19–24, [nucl-th/9711011].
- [28] S. Mrówczyński and P. Słoń, *Hadron-Deuteron Correlations and Production of Light Nuclei in Relativistic Heavy-ion Collisions*, *Acta Phys. Polon. B* **51** (2020), no. 8 1739–1755, [arXiv:1904.08320].
- [29] S. Bazak and S. Mrowczynski, *Production of ^4Li and $p-^3\text{He}$ correlation function in relativistic heavy-ion collisions*, *Eur. Phys. J. A* **56** (2020), no. 7 193, [arXiv:2001.11351].
- [30] P. Danielewicz and G. F. Bertsch, *Production of deuterons and pions in a transport model of energetic heavy ion reactions*, *Nucl. Phys.* **A533** (1991) 712–748.
- [31] D. Oliinychenko, L.-G. Pang, H. Elfner, and V. Koch, *Microscopic study of deuteron production in PbPb collisions at $\sqrt{s} = 2.76\text{TeV}$ via hydrodynamics and a hadronic afterburner*, *Phys. Rev.* **C99** (2019), no. 4 044907, [arXiv:1809.03071].
- [32] S. Samanta and F. Giacosa, *QFT treatment of a bound state in a thermal gas*, *Phys. Rev. D* **102** (2020) 116023, [arXiv:2009.13547].
- [33] F. Giacosa and G. Pagliara, *On the spectral functions of scalar mesons*, *Phys. Rev. C* **76** (2007) 065204, [arXiv:0707.3594].
- [34] W. Weinhold, B. Friman, and W. Noerenberg, *Thermodynamics of an interacting πN system*, *Acta Phys. Polon. B* **27** (1996) 3249–3253.
- [35] W. Weinhold, B. Friman, and W. Noerenberg, *Thermodynamics of Delta resonances*, *Phys. Lett. B* **433** (1998) 236–242, [nucl-th/9710014].
- [36] W. Florkowski, *Phenomenology of Ultra-Relativistic Heavy-Ion Collisions*. World Scientific, Singapore, 2010.
- [37] W. Broniowski, F. Giacosa, and V. Begun, *Cancellation of the σ meson in thermal models*, *Phys. Rev. C*

- 92** (2015), no. 3 034905, [arXiv:1506.01260].
- [38] P. M. Lo, B. Friman, K. Redlich, and C. Sasaki, *S-matrix analysis of the baryon electric charge correlation*, *Phys. Lett. B* **778** (2018) 454–458, [arXiv:1710.02711].
- [39] P. M. Lo and F. Giacosa, *Thermal contribution of unstable states*, *Eur. Phys. J. C* **79** (2019), no. 4 336, [arXiv:1902.03203].
- [40] P. M. Lo, M. Marczenko, K. Redlich, and C. Sasaki, *Matching the Hagedorn mass spectrum with Lattice QCD results*, *Phys. Rev. C* **92** (2015), no. 5 055206, [arXiv:1507.06398].
- [41] P. M. Lo, B. Friman, M. Marczenko, K. Redlich, and C. Sasaki, *Repulsive interactions and their effects on the thermodynamics of a hadron gas*, *Phys. Rev. C* **96** (2017), no. 1 015207, [arXiv:1703.00306].
- [42] M. E. Peskin and D. V. Schroeder, *An Introduction to quantum field theory*. Addison-Wesley, Reading, USA, 1995.
- [43] A. Messiah, *Quantum Mechanics*. Dover Publication, New York, USA, 1999.
- [44] W. R. Frazer, *Dynamical Models Based on Unitarity and Analyticity*, in *Summer School in Elementary Particle Physics: Theories of strong interactions at high energies* (H. J. Yesian, ed.), 1969.
- [45] J. R. E. Taylor, *Scattering Theory: The Quantum Theory of Nonrelativistic Collisions*. John Wiley, USA, 1972.
- [46] F. Giacosa, A. Pilloni, and E. Trozzi, *Glueball-glueball scattering and the glueballonium*, arXiv:2110.05582.
- [47] J. B. Hartle and C. E. Jones, *Inelastic Levinson's theorem, cdd singularities and multiple resonance poles*, *Annals Phys.* **38** (1966) 348–362.
- [48] M. Wellner, *Levinson's Theorem (an Elementary Derivation)*, *American Journal of Physics* **32**.
- [49] R. Dashen, S.-K. Ma, and H. J. Bernstein, *S Matrix formulation of statistical mechanics*, *Phys. Rev.* **187** (1969) 345–370.
- [50] R. Venugopalan and M. Prakash, *Thermal properties of interacting hadrons*, *Nucl. Phys. A* **546** (1992) 718–760.
- [51] P. M. Lo, *S-matrix formulation of thermodynamics with N-body scatterings*, *Eur. Phys. J. C* **77** (2017), no. 8 533, [arXiv:1707.04490].
- [52] A. Dash, S. Samanta, and B. Mohanty, *Interacting hadron resonance gas model in the K -matrix formalism*, *Phys. Rev. C* **97** (2018), no. 5 055208, [arXiv:1802.04998].
- [53] A. Dash, S. Samanta, and B. Mohanty, *Thermodynamics of a gas of hadrons with attractive and repulsive interactions within an S -matrix formalism*, *Phys. Rev. C* **99** (2019), no. 4 044919, [arXiv:1806.02117].
- [54] X.-Q. Luo, Y.-Y. Li, and H. Kroger, *Bound states and critical behavior of the Yukawa potential*, *Sci. China G* **35** (2005) 631–642, [hep-ph/0407258].
- [55] M. Napsuciale and S. Rodriguez, *Complete analytical solution to the quantum Yukawa potential*, *Phys. Lett. B* **816** (2021) 136218, [arXiv:2012.12969].
- [56] G. D. Yen, M. I. Gorenstein, W. Greiner, and S.-N. Yang, *Excluded volume hadron gas model for particle number ratios in A+A collisions*, *Phys. Rev. C* **56** (1997) 2210–2218, [nucl-th/9711062].
- [57] V. Baru, J. Haidenbauer, C. Hanhart, Y. Kalashnikova, and A. E. Kudryavtsev, *Evidence that the $a(0)(980)$ and $f(0)(980)$ are not elementary particles*, *Phys. Lett. B* **586** (2004) 53–61, [hep-ph/0308129].
- [58] K. Hayashi, M. Hirayama, T. Muta, N. Seto, and T. Shirafuji, *Compositeness criteria of particles in quantum field theory and S-matrix theory*, *Fortsch. Phys.* **15** (1967), no. 10 625–660.
- [59] Y.-b. Dong, A. Faessler, T. Gutsche, and V. E. Lyubovitskij, *Phenomenological Lagrangian approach to the electromagnetic deuteron form factors*, *Phys. Rev. C* **78** (2008) 035205, [arXiv:0806.3679].